Cold Regions Science and Technology 206 (2023) 103738

Contents lists available at ScienceDirect

Cold Regions Science and Technology

journal homepage: www.elsevier.com/locate/coldregions

# Low temperature performances of fiber-reinforced asphalt mixtures for surface, binder, and base layers

Chiara Riccardi [a,1], Irune Indacoechea [b], Di Wang [c,*,1], Pedro Lastra-González [b], Augusto Cannone Falchetto [c,*], Daniel Castro-Fresno [b]

[a] Department of Civil and Industrial Engineering, University of Pisa, Largo L. Lazzarino, 1, 56122 Pisa, Italy
[b] GITECO Research Group, Universidad de Cantabria, Avda. de Los Castros s/n., 39005 Santander, Spain
[c] Department of Civil Engineering, Rakentajanaukio 4, 02150 Espoo, Finland, Aalto University, Finland

ARTICLE INFO

*Keywords:*
Fiber reinforced porous asphalt and asphalt mixture
Aramid
Polyolefins and polyacrylonitrile fibers
RAP
Low temperatures performance properties
Thermal cracking
Thermal fracture

ABSTRACT

In the present study, the effects of adding fibers and Reclaimed Asphalt Pavement (RAP) on the low temperature performances of open graded asphalt mixtures for surface layer and dense asphalt mixtures for surface, binder, and base layers were investigated. Two different kinds of fibers were used: a combination of aramid and polyolefins fibers were utilized for preparing fiber reinforced porous asphalt mixtures, while polyacrylonitrile fibers were employed for producing conventional dense asphalt mixtures for surface, binder, and base layers. Reference mixtures were made with virgin materials as a benchmark to study the effects of the fibers' addition. Moreover, asphalt mixtures for surface layers composed of 30% RAP and mixtures for binder layers containing 50% RAP were produced to study the combined effects of fibers and RAP on the low temperature's performance. Thermal Stress Restrained Specimen, Uniaxial Tension Stress, and Semi-Circular Bending tests were used to evaluate the response against thermal distresses. The addition of the fibers showed no significant effects on the low temperature strength, while a remarkable improvement in the failure temperature and crack propagation resistance properties was found. The use of fibers has also shown to be beneficial in combination with mixtures designed with RAP and higher binder content suggesting a dedicated study on mix design for future research.

## 1. Introduction

Transport infrastructure plays a vital role in a country's economic growth by allowing the mobilization of citizens and goods and thus providing access to jobs, health, education, and leisure and facilitating trade between regions, countries, and continents. However, the continuous increase in heavy traffic and the extreme events associated with climate change can rapidly deteriorate the road infrastructure, drastically reducing its service life (Li et al., 2011; Office et al., 2021). Scientists and engineers are constantly looking for novel materials and technologies to increase the asphalt mixtures' durability and resilience (Wang et al., 2018; Slebi-Acevedo et al., 2020a; Wang et al., 2021). Among the different technologies, several research works have demonstrated that the addition of different types of fibers to asphalt mixtures can result in better performance properties in both Asphalt Concrete (AC) and Porous Asphalt (PA) (Abtahi et al., 2010; Gupta et al., 2019; Slebi-Acevedo et al., 2019). In addition, the use of fibers has shown potentially environmental benefits due to the dry process of adding fibers at ambient temperature. Hence, using fibers in substitution for polymers could help save a significant amount of greenhouse gas (GHG) emissions and energy during the production of asphalt mixtures (Achilleos et al., 2011).

## 2. Research background

For fiber-reinforced asphalt mixtures (FRAM) prepared with fresh materials, Kaloush et al. (2010) evaluated the mechanical properties of AC mixtures reinforced with a blend of polyolefin-aramid fibers. The authors reported a remarkably positive effect of the mixture's rutting resistance and an increment of 25–50% in the tensile strengths and 50–75% in fracture energies. Similarly, Xu et al. (2010) found that AC mixtures reinforced with polyester and polyacrylonitrile present higher

* Corresponding authors.
*E-mail addresses:* chiara.riccardi@unipi.it (C. Riccardi), irune.indacoechea@unican.es (I. Indacoechea), di.1.wang@aalto.fi (D. Wang), pedro.lastragonzalez@unican.es (P. Lastra-González), augusto.cannonefalchetto@aalto.fi (A. Cannone Falchetto), daniel.castro@unican.es (D. Castro-Fresno).
[1] formerly at Technical University of Braunschweig, Beethovenstraße 51b, 38,106 Braunschweig, Germany.

https://doi.org/10.1016/j.coldregions.2022.103738
Received 24 July 2022; Received in revised form 15 November 2022; Accepted 26 November 2022
Available online 1 December 2022

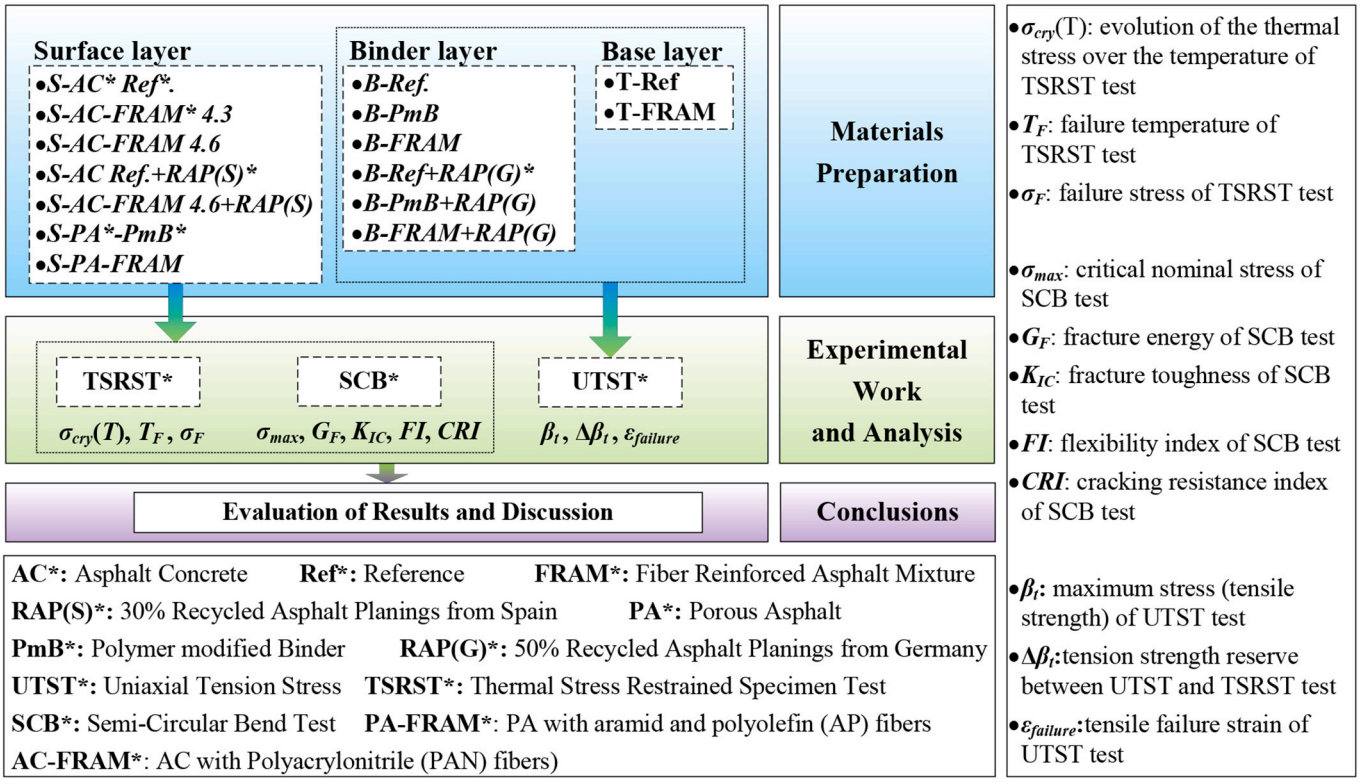


**Fig. 1.** Research approach.

**Table 1**
Binders' conventional properties.

| Binder types | Penetration [dmm] | Softening point temperature [°C] |
|---|---|---|
| 50/70 from Germany | 58 | 48.2 |
| 40/100–65 from Germany | 64 | 75.0 |
| 35/50 from Germany | 35 | 56.6 |
| RAP binder from Germany | 19 | 65.0 |
| 50/70 from Spain | 57 | 51.6 |
| 45/80–65 from Spain | 55 | 74.1 |
| RAP binder from Spain | 6 | 71.9 |

values of rutting resistance, fatigue life, and indirect tensile strength (ITS). In another research work, Mahrez et al. (2005) studied the impact of adding glass fiber to stone matrix asphalt (SMA), reporting the potential of the fibers to enhance rutting and cracking resistance. Although to a much lower extent, the fiber reinforcement of PA mixtures has also been investigated. In this sense, Slebi-Acevedo et al. (2020b) studied the impact of adding two different types of fibers to PA mixtures (a blend of polyolefin-aramid and polyacrylonitrile). According to the authors, the addition of fibers increased the ductility of the PA mixture, improving the overall toughness of the material. Punith and Veeraragavan (2011) also evaluated the effect of adding fibers to PA mixes. In this case, waste polyethylene (PE) fibers were incorporated into open graded friction course (OGFC) mixtures. Results indicated that the addition of PE fibers improved the tensile strength and the resistance to moisture sensitivity and fatigue damage. Some researchers also worked on the influence of fiber in asphalt mixture containing RAP. It was found that different types of fiber can ultimately lead to an increment in moisture, fatigue, and rutting resistance performance in asphalt mixtures containing high content of RAP (Fakhri and Hosseini, 2017; Wu et al., 2020; Ziari et al., 2020, 2021). In Europe, up to 50% RAP can be recognized as high RAP

**Table 2**
Asphalt mixture types.

| Mixture | Binder type | Aggregate type | Binder content [%] | Fiber content [%] | Void content [%] |
|---|---|---|---|---|---|
| *S-AC Ref.* | 50/70 | Ophite coarse aggregates+ limestone fines and filler | 4.3 | 0 | 5.1 |
| *S-AC-FRAM 4.3* | 50/70 | | 4.3 | 0.15 | 6.2 |
| *S-AC-FRAM 4.6* | 50/70 | | 4.6 | 0.15 | 5.6 |
| *S-AC Ref. + RAP (S)* | 50/70 + RAP | | 3.5 + 1.5 RAP | 0 | 4.9 |
| *S-AC-FRAM 4.6 + RAP(S)* | 50/70 + RAP | | 3.5 + 1.5 RAP | 0.15 | 4.0 |
| *S-PA-PmB* | 45/80–65 | Gabbro+ limestone filler | 4.5 | 0 | 21.4 |
| *S-PA-FRAM* | 50/70 | | 5 | 0.05 | 20.4 |
| *B-Ref.* | 50/70 | | 4.4 | 0 | 5.8 |
| *B-PmB* | 40/100–65 | | 4.4 | 0 | 5.5 |
| *B-FRAM* | 50/70 | | 4.4 | 0.15 | 5.0 |
| *B-Ref + RAP(G)* | 50/70 + RAP | | 2.3 + 2.1 RAP | 0 | 5.5 |
| *B-PmB + RAP(G)* | 40/100–65 + RAP | | 2.3 + 2.1 RAP | 0 | 5.2 |
| *B-FRAM + RAP (G)* | 50/70 + RAP | | 2.3 + 2.1 RAP | 0.15 | 4.3 |
| *T-Ref.* | 50/70 | Gabbro+ limestone filler | 4 | 0 | 6.5 |
| *T-FRAM* | 35/50 | | 4 | 0.15 | 6.3 |

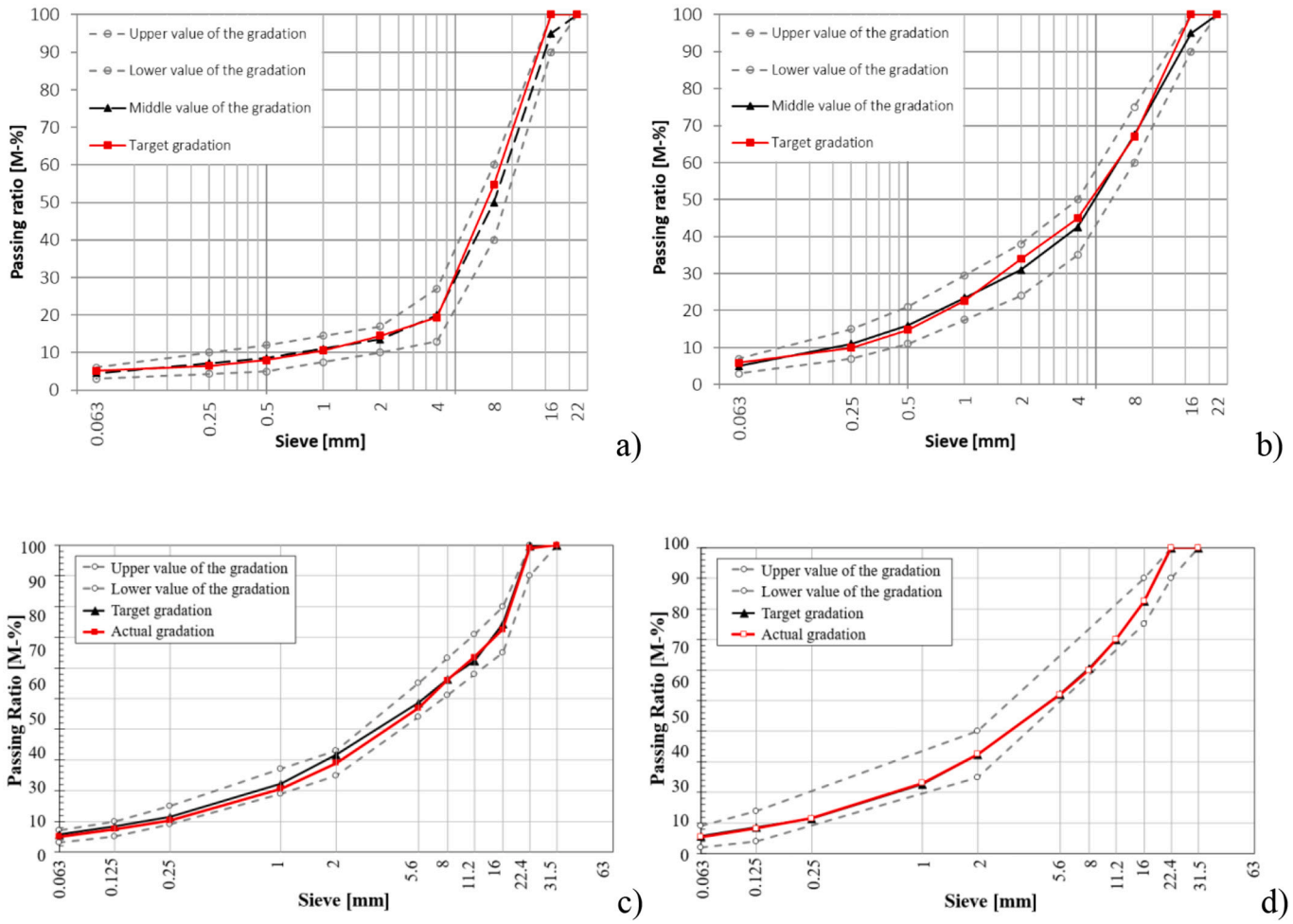


**Fig. 2.** Grading curve used for: (a) porous asphalt mixtures; (b) asphalt concrete for surface layer; (c) binder layer, and (d) base layer.

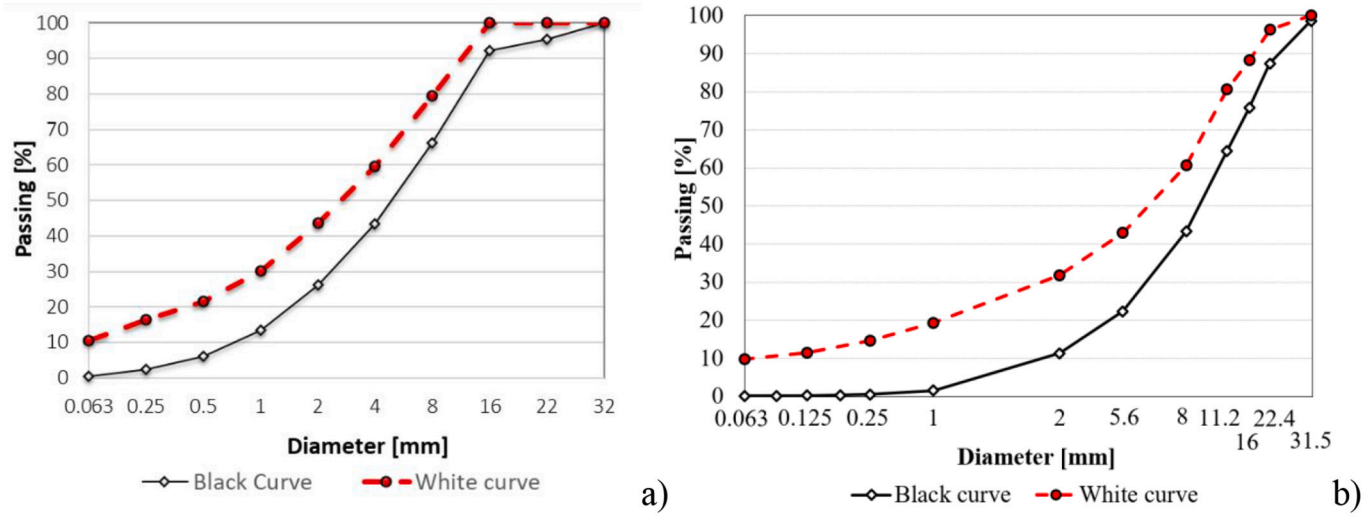


**Fig. 3.** Black and white curves of the RAP: (a) Spanish source; (b) German source.

content (EAPA, 2022; Hugener et al., 2022). Hence, it was validated that the use of fiber could reinforce the performance properties of AC and PA mixtures, with and without RAP, at intermediate and high temperatures.

However, concerning the resistance to low-temperature cracking and fracture properties of FRAM, no consistent results could be achieved regardless of the use of RAP. For unaged AC and PA mixtures, Park et al. (2015) evaluated the impact of steel fibers on AC mixtures by performing indirect tensile strength (ITS) at −20 °C. Significant enhancement in thermal cracking resistance was found with an improvement of 62.5% in ITS and up to 370% in fracture energy. Similarly, Morea and

**Table 3**
Characteristics of the aramid and polyolefin fibers.

| Characterization | AP fibers | PAN fibers |
|---|---|---|
| | Description or parameters | |
| Form | Monofilament (A)/ Serrated (P) | staple fibers |
| Appearance | Yellow (A)/Yellow (A) | bright straw yellow gold |
| Density [g/cm$^3$] | 1.44 (A)/0.91 (P) | 1.18 |
| Humidity [%] | – | <2 or 18 |
| Tensile strength [MPa] | >2758(A) />483 (P) | |
| Tenacity [MPa] | – | >708 |
| Elastic modulus [MPa] | – | 16,500 |
| Elongation at break [%] | – | <13 |
| $T_g$[a] in air [°C] | – | 100 |
| $T_m$ in air [°C] | – | 330 |
| Chemical resistance | Acid/Alkali inert (A) / Acid/Alkali inert (P) | all chemicals except Dimethylacetamide (DMAC); Dimethyl sulfoxide (DMSO); Dimethylformamide (DMF); $ZnCl_2$; Sodium thiocyanate (NaSCN) |
| Other resistance | – | Ultraviolet (UV), rot and weathering |

[a] $T_g$: glass transition temperature.

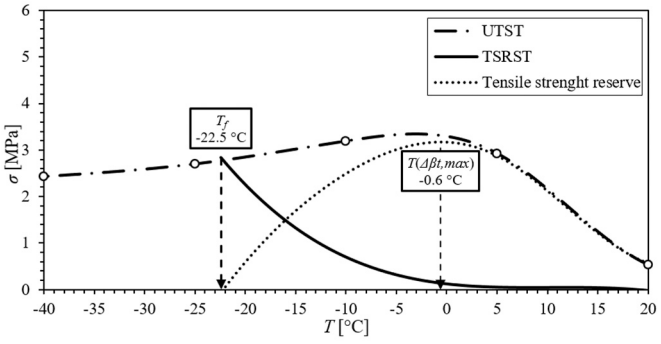


**Fig. 4.** Illustration of tensile strength reserve calculation.

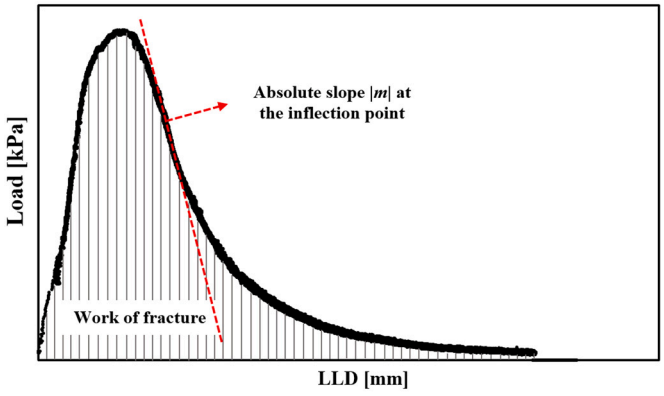


**Fig. 5.** Illustration of tensile strength reserve calculation.

Zerbino (2018) used the notched beam bending test to analyze the effect of glass fibers in AC mixtures. An improved thermal fracture property was found compared to the reference mixture. For AC mixtures containing RAP up tp 50% (Wu et al., 2020), higher fracture energy was observed in the basalt fiber prepared FRAM with different RAP contents than the reference mixture by using semi-circular bending (SCB) test. Muftah et al. (2017) and Bayomy et al. (2016) studied the effect of

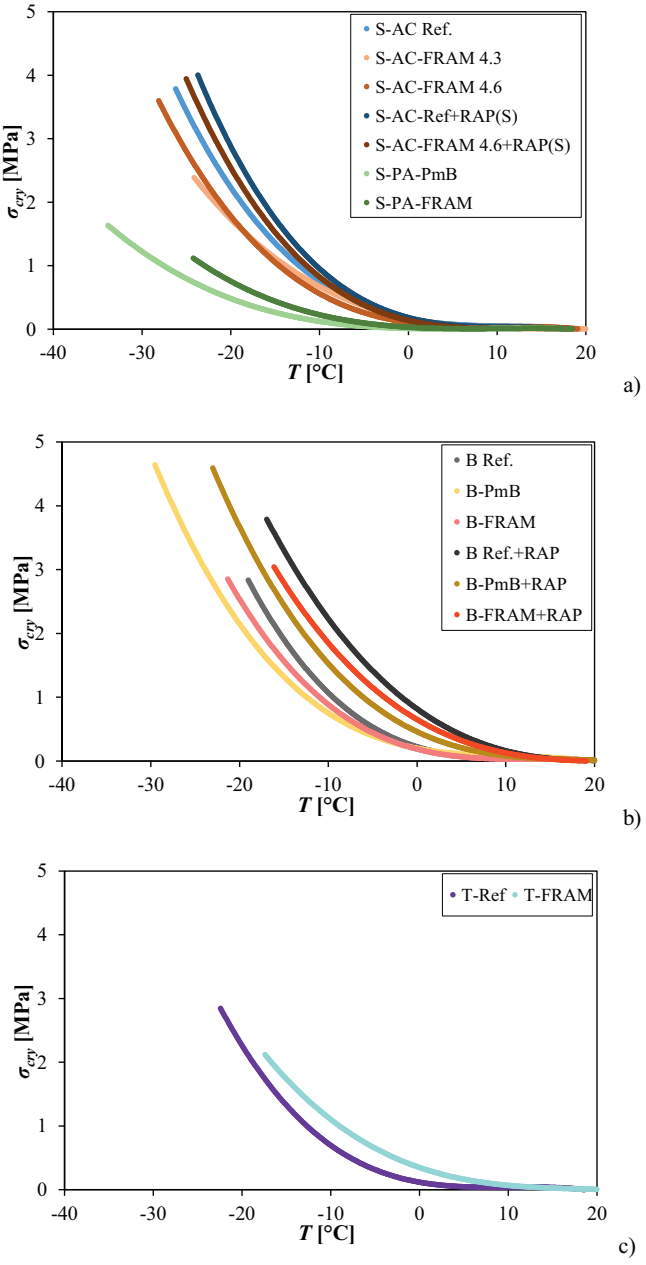


**Fig. 6.** Thermal stress versus temperature for a) surface layers' mixtures; b) binder layers' mixtures; and c) base layers' mixtures.

aramid and polyethylene fibers on AC mixture containing 47% RAP in Idaho State, USA. The low temperature properties were evaluated by Indirect tensile tests (IDT) at −20 °C and − 10 °C. No significant differences with even slightly worse properties were observed in the FRAM compared to the reference mixtures at the fiber content given by the supplier. Different fiber contents were suggested to be used to find the optimal mix design.

In conclusion, many studies have been conducted on the mechanical and performance properties of FRAM with and without RAP. An overall improvement could be achieved at high and intermediate temperatures. However, the low temperature behavior of FRAM composed with high RAP contents appears to be still not fully understood, particularly in the case of asphalt materials prepared with aramid and polyolefin fibers with different mix designs.

**Table 4**
TSRST results.

| Mixtures | Failure temperature $T_F$ [°C] | SD | Failure stress $\sigma_F$ [MPa] | SD |
|---|---|---|---|---|
| *S-AC Ref.* | −26.2 | 0.59 | 3.723 | 0.15 |
| *S-AC-FRAM 4.3* | −24.2 | 0.72 | 2.300 | 0.03 |
| *S-AC-FRAM 4.6* | −28.2 | 0.43 | 3.474 | 0.06 |
| *S-AC Ref. + RAP(S)* | −23.7 | 0.81 | 3.915 | 0.19 |
| *S-AC-FRAM 4.6 + RAP(S)* | −25.1 | 0.65 | 3.817 | 0.26 |
| *S-PA-PmB* | −33.8 | 0.42 | 1.690 | 0.06 |
| *S-PA-FRAM* | −24.2 | 0.54 | 1.114 | 0.06 |
| *B-Ref* | −19.1 | 0.73 | 2.833 | 0.26 |
| *B-PmB* | −29.5 | 0.82 | 4.638 | 0.23 |
| *B-FRAM* | −21.4 | 0.83 | 2.848 | 0.17 |
| *B-Ref + RAP* | −16.9 | 0.37 | 3.785 | 0.09 |
| *B-PmB + RAP* | −23.0 | 0.82 | 4.591 | 0.17 |
| *B-FRAM + RAP* | −16.2 | 0.70 | 3.039 | 0.21 |
| *T-Ref* | −22.5 | 0.67 | 2.845 | 0.18 |
| *T-FRAM* | −17.5 | 0.53 | 2.120 | 0.23 |

SD: Standard deviation.

## 3. Objectives and research approaches

In the present study, low temperature performances of fiber reinforced asphalt mixtures (FRAM) for surface, binder, and base layers were studied by using different testing methods: Thermal Stress Restrained Specimen Test (TSRST) (EN 12697-46, 2012), Uniaxial Tension Stress Test (UTST) (EN 12697-46, 2012), and Semi-Circular Bending test (SCB) (EN 12697-44, 2019). The results were compared to reference mixtures composed of fresh materials to estimate the effects of the addition of the fibers and to polymer-modified mixtures to determine if FRAMs can provide similar performance. In addition, since the use of Reclaimed Asphalt Pavement (RAP) is nowadays a common environmental friendly practice (Aurangzeb et al., 2014; Büchler et al., 2018), the potential effects of fibers on the low temperature performances of asphalt mixtures with high RAP content (30% by total weight for the surface layer mixture, and 50% for the binder layer mixture) were investigated. The research approach is summarized in Fig. 1.

## 4. Materials and testing

### 4.1. Material

Five different binders: two different sources of 50/70 (one from Germany and the other one from Spain), a 35/50 Pen Grade (EN 12591, 2015), and polymer modified binders 40/100–65 and 45/80–65 (EN 14023, 2010) were used to produce a set of fifteen mixtures for surface (*S*), binder (*B*) and base (*T*) layers. The characteristics of the binders, including the extracted binders (EN 12697-3, 2013) from the Spanish and German RAP sources, are summarized in Table 1.

Ten asphalt mixtures (Table 2) were prepared with fresh materials only: five of them for the surface layers (*S*), three for binder layers (*B*), and two for base layers (*T*).

For the surface layers, two different types of mixtures were produced in Spain according to the Spanish specifications (Ministerio de Fomento, 2010): Asphalt Concrete (AC) and Porous Asphalt (PA). The binder (B) and base layers' (T) mixtures (produced in Germany) were fabricated following the German specifications (TL Asphalt-StB 07/13, 2013) for the mix design.

All the acronyms used for the different mixtures and their composition (binders', aggregates' and fibers' types; binders', fibers', and voids' contents are all summarized in Table 2. Different optimal fibers were selected in the authors' previous studies for PA and AC mixtures, respectively (Kim et al., 2020; Slebi-Acevedo et al., 2021). All the fiber contents are suggested by the producers.

In addition, four mixtures for surface layers were prepared by replacing 30% of the total weight with RAP obtained in Spain (RAP(S)) from a fifteen year old surface course of a local road. Three mixtures for the binder layer were produced with 50% recycled materials originating from a RAP source in Germany (RAP(G)) from a ten-year-old binder course. These mixtures were identified as S-AC Ref. + RAP(S), S-AC-FRAM 4.6 + RAP(S), B-Ref + RAP(G), B-PmB + RAP(G), and B-FRAM+RAP(G).

The mixtures have the same gradation curve as reported in Fig. 2a, b, c, and d, typically used for surface, binder, and base layers, respectively.

The physical and geometrical properties of the RAP source were also investigated. In particular, the black and white curves reported in Fig. 3 were determined following EN 12697-2 (2013) and EN 13108-1 (2016). The aggregate gradation of RAP after water washing over a 0.063 mm sieve to remove the finest particles can be defined as the "black curve", while the aggregate gradation obtained after binder recovery was determined as the "white curve" of RAP (EN 933-1, 2012). Then, the binder content of the RAP aggregates was determined on five samples with the rotatory evaporator (EN 12697-3, 2013) and resulted in 4.93% for the German RAP source and 5.10% for the Spanish RAP source. German and Spanish RAP sources' specific gravity (EN 12697-5, 2019) was 2.925 g/cm$^3$ and 2.522 g/cm$^3$, respectively.

The properties of the fibers used in the present work are summarized in Table 3. The nominal length and diameter of the PAN fiber were 4 mm and 10 μm, respectively. In the case of AP fibers, the length of the aramid and polyolefin fibers is the same, 19 mm. More information on the thermal and chemical properties of these fibers (both type AP and PAN) and of the microstructure of fibers incorporation within the mixtures can be found in Bueno and Poulikakos (2020).

### 4.2. Testing

To better understand the low temperature performances of the mixtures containing fibers and of those containing both fibers and RAP, different testing protocols were used: Thermal Stress Restrained Specimen (TSRST) (EN 12697-46, 2012), Uniaxial Tension Stress (UTST) (EN 12697-46, 2012) and Semi-Circular Bending (SCB) tests (EN 12697-44, 2019).

#### 4.2.1. Thermal stress restrained specimen test (TSRST)

TSRST was performed in accordance with EN 12697-46 (2012) on prismatic asphalt specimens with dimensions of 50 × 50 × 160 mm$^3$. The sample is held at a constant length during the test while its temperature decreases from a starting temperature of +20 °C, with a cooling rate $\Delta T = -10$ K/h. Due to the prevented thermal shrinkage, the specimen is subjected to an increasing (cryogenic) tensile stress. The test ended at a minimum test temperature of $T = -40$ °C or at failure when the cryogenic stress reached the tensile strength of the asphalt sample. The TSRST results include the evolution of the cryogenic (thermal) tensile stress over the temperature $\sigma_{cry}(T)$, the failure stress $\sigma_F$, and the failure temperature $T_F$. The failure stress is equivalent to the strength of the specimen at the failure temperature.

#### 4.2.2. Uniaxial tension stress (UTST)

To assess the strength properties of the asphalt mixtures at low temperatures, UTST was performed in accordance with EN 12697-46 (2012) on prismatic samples with dimensions of 50 × 50 × 160 mm$^3$. During the test, the specimen is pulled at a constant strain rate of 0.625%/min, corresponding to a tension rate of 1 mm/min, at a constant temperature until failure. Four temperatures (−25 °C, −10 °C, 5 °C, 20 °C) were investigated, and three samples for each temperature were tested.

The results of the UTST consist of the maximum stress (tensile strength) $\beta_t(T)$, and the corresponding tensile failure strain $\varepsilon_{failure}(T)$ at the testing temperature *T*. Moreover, based on both results of TSRST and UTST, the tension strength reserve $\Delta\beta_t(T)$ for each asphalt mixture was derived using Eq. (1):

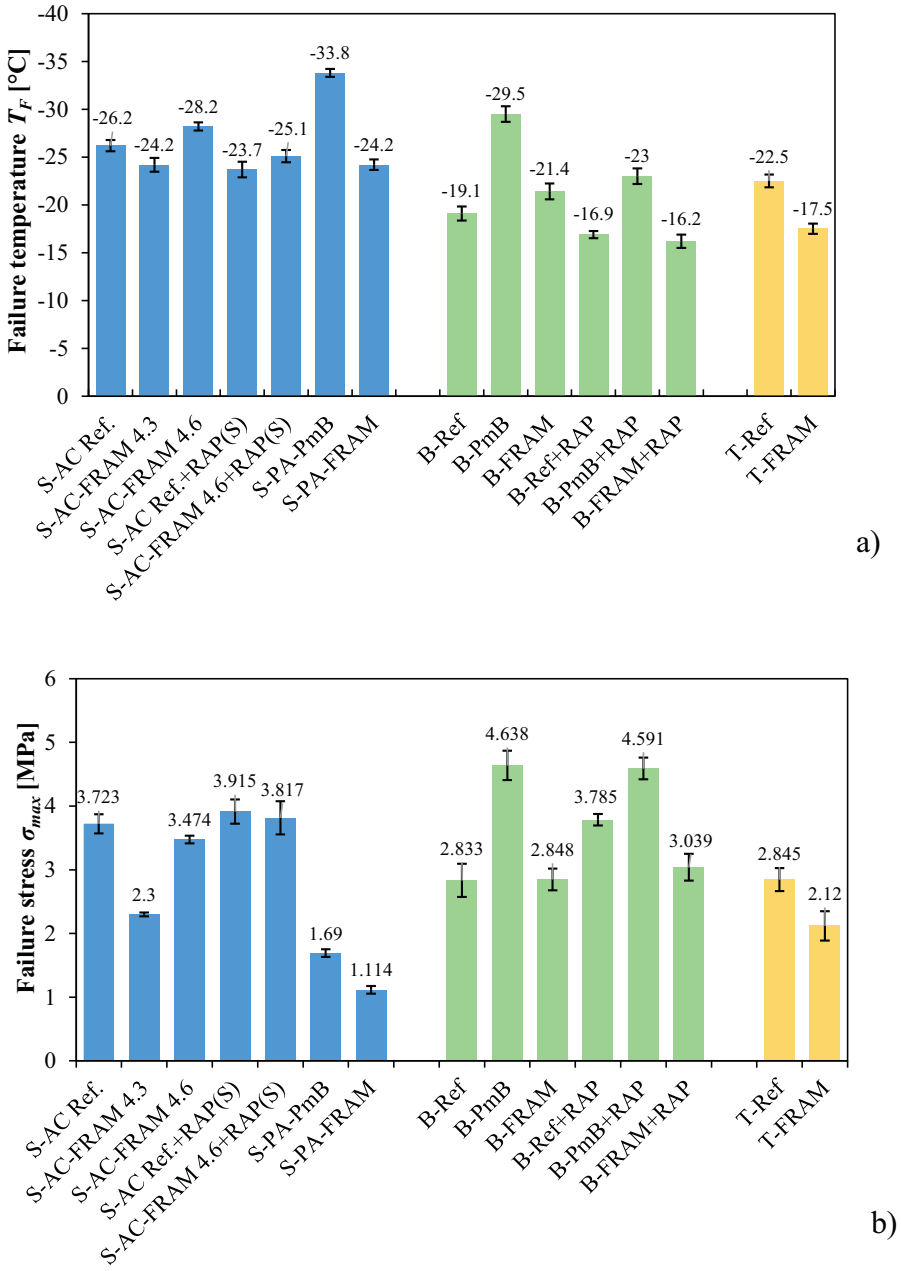


**Fig. 7.** TSRST results and the standard deviation for a) failure temperature $T_F$; and b) failure stress $\sigma_F$.

**Table 5**
Categories for maximum failure temperature $TSRST_{max}$ (EN 13108-1, 2016).

| Maximum failure temperature [°C] | Category $TSRST_{max}$ | Maximum failure temperature [°C] | Category $TSRST_{max}$ |
|---|---|---|---|
| −15.0 | $TSRST_{max-15.0}$ | −25.0 | $TSRST_{max-25.0}$ |
| −17.5 | $TSRST_{max-17.5}$ | −27.5 | $TSRST_{max-27.5}$ |
| −20.0 | $TSRST_{max-20.0}$ | −30.0 | $TSRST_{max-30.0}$ |
| −22.5 | $TSRST_{max-22.5}$ | | |

**Table 6**
Cold region classification system for surface, binder, and base layer's mixture based on the failure temperature $T_F$ according to RStO 01 (2012).

| Cold region classification | Surface and binder layers' mixture | Base layer mixture |
|---|---|---|
| I | $T_F \leq -15$ °C | $T_F \leq -10$ °C |
| II | $T_F \leq -20$ °C | $T_F \leq -15$ °C |
| III | $T_F \leq -25$ °C | $T_F \leq -20$ °C |

$$\Delta\beta_t(T) = \beta_t(T) - \sigma_{cry}(T) \quad (1)$$

The maximum value of this reserve is an important parameter helpful in understanding the low-temperature properties of asphalt mixtures in terms of thermal stresses and traffic loads. It is the reserve that is available for accommodating additional superimposed stresses.

Based on the results of the TSRST and UTST tests, it is possible to calculate the tensile strength reserve using Eq. (1). An example of tensile strength reserve analysis is presented in Fig. 4, which shows the cryogenic stress (TSRST) results and the tensile strength (UTST) versus temperature with the curve that is the final result of tensile strength reserve calculations. (See Fig. 5.)

**Table 7**
Classification of the mixtures (RStO 01, 2012; EN 13108-1, 2016) .

| Mixtures | EN 13108-1 (2016) | RStO 01 (2012) |
|---|---|---|
| *S-AC Ref.* | $TSRST_{max-25.0}$ | III |
| *S-AC-FRAM 4.3* | $TSRST_{max-22.5}$ | II |
| *S-AC-FRAM 4.6* | $TSRST_{max-27.5}$ | III |
| *S-AC Ref. + RAP(S)* | $TSRST_{max-22.5}$ | II |
| *S-AC-FRAM 4.6 + RAP(S)* | $TSRST_{max-25.0}$ | III |
| *S-PA-PmB* | $TSRST_{max-30.0}$ | III |
| *S-PA-FRAM* | $TSRST_{max-22.5}$ | II |
| *B-Ref* | $TSRST_{max-17.5}$ | I |
| *B-PmB* | $TSRST_{max-27.5}$ | III |
| *B-FRAM* | $TSRST_{max-20.0}$ | II |
| *B-Ref + RAP* | $TSRST_{max-15.0}$ | I |
| *B-PmB + RAP* | $TSRST_{max-22.5}$ | II |
| *B-FRAM + RAP* | $TSRST_{max-15.0}$ | I |
| *T-Ref* | $TSRST_{max-22.5}$ | III |
| *T-FRAM* | $TSRST_{max-17.5}$ | II |

#### 4.2.3. Semi-circular bending test (SCB)

Semi-Circular Bending tests were used to evaluate the fracture properties of the mixture at low temperatures. The adopted procedure relies on methods proposed in previous studies (Zegeye, 2012; Cannone Falchetto et al., 2017a; Cannone Falchetto et al., 2018; AASHTO T394, 2021). The testing geometry consists of a semi-circular sample having a diameter of 150 mm and a thickness of 30 mm, and a 15 mm deep notch is fabricated at the bottom central flat part of the specimen. Loading is controlled and adjusted by a closed-loop system through Load Line Displacement (LLD) and Crack Mouth Opening Displacement (CMOD) sensors. Two testing temperatures were considered for the experimentation on all materials: −18 °C and − 24 °C; each testing condition was replicated three times. For the loading protocol, an initial load of 1 kN was reached in the first ten seconds, then, the loading mode was changed to CMOD control. Optimal loading rates were selected for different testing temperatures based on the authors' previous studies (Cannone Falchetto et al., 2018; Al-Qudsi et al., 2020).

Based on EN 12697-44 (2019), the critical nominal stress $\sigma_{max}$, and two main fracture parameters, fracture energy, $G_F$, and fracture toughness can be calculated by using the following equations:

$$G_F = W_F \Big/ A_{lig} = \int P du \Big/ A_{lig} \tag{2}$$

$$K_{Ic} = \sigma_{\max} \cdot Y_I \tag{3}$$

$$Y_I = -4.9965 + 155.58\left(\frac{a}{r}\right) - 799.94\left(\frac{a}{r}\right)^2 + 2141.9\left(\frac{a}{r}\right)^3 - 2709.1\left(\frac{a}{r}\right)^4 + 1398.6\left(\frac{a}{r}\right)^5 \tag{4}$$

Moreover, two additional fracture parameters: Illinois Flexibility Index, *FI* (Yan et al., 2020), and Cracking Resistance Index, *CRI* (Moghaddam et al., 2014), were calculated to better understand the fracture responsed of SCB samples:

$$FI = G_F/|m| \times A = G_F/|m| \times 0.01 \tag{5}$$

$$CRI = G_F/P_{\max} \tag{6}$$

where $W_F$ is the work of fracture; $A_{lig}$ is the ligament area, given by $A_{lig} = (r\text{-}a) \times t$; the division of $W_F$ and $A_{lig}$ is the fracture energy $G_F$; $Y_I$ is the normalized stress intensity factor (dimensionless); $\sigma_{max}$ equals to $P_{max}/(2{\cdot}r{\cdot}t)$, where $P_{max}$ is the peak load; $a$ is the notch length; $r$ is the radius or the height of the sample and $t$ is the sample thickness; $m$ is the absolute slope of the inflection point on the load-displacement curve after the post peak curve (Fig. 3); $A$ is a scaling constant taken to be 0.01 for laboratory compacted samples.

As shown in Eq. (3), $\sigma_{max}$ is the nominal stress obtained at the peak load. $K_{Ic}$ is the stress intensity factor at the critical load (peak load), representing the highest value of stress intensity factor that the material can bear without fracture; it quantifies the ability of the materials to resist cracking. Commonly macro-cracking occurs when the material reaches the peak load. Hence, both $\sigma_{max}$ and $K_{Ic}$ can quantitatively reflect the asphalt mixtures' cracking resistance. The calculation of $G_F$ is the area under the load vs. load line displacement (LLD) curve by the ligament area (the product of the ligament length and the thickness of the specimen) of the SCB specimen prior to testing (EN 12697-44, 2019). Considering the curve shape, the value of $G_F$ highly relies on the mixture's behavior after load peak. A brittle material with a sharp decreasing curve may lead to a lower $G_F$, while more plastic-like materials exhibit a wider post-peak, ultimately resulting in a higher $G_F$. In a viscoelastic material such as asphalt mixture, the fracture energy increases with crack growth. Such increase does not rely on crack length or growth rate; it only depends on the work needed for crack propagation. Hence, a higher value of $G_F$ means higher energy required to fracture the sample and indicates better fracture resistance. The parameters $\sigma_{max}$ and $K_{Ic}$ are used to evaluate the resistance cracking properties before a macro-crack occurs, while $G_F$ is used to assess the resistance to crack propagation after macro-cracking (Cannone Falchetto et al., 2018; AASHTO T394, 2021).

**Table 8**
UTST results.

| Mixtures | | Tensile strenght, $\beta_t$ [MPa] | | | | Tensile failure strain, $\varepsilon_{failure}$ [MPa] | | | |
|---|---|---|---|---|---|---|---|---|---|
| | | -25 °C | −10 °C | 5 °C | 20 °C | −25 °C | −10 °C | 5 °C | 20 °C |
| *B-Ref.* | mean value | 2.191 | 2.263 | 2.823 | 0.532 | 0.364 | 0.174 | 0.879 | 4.590 |
| | st.deviation | 0.257 | 0.122 | 0.075 | 0.003 | 0.031 | 0.020 | 0.018 | 0.531 |
| *B-PmB* | mean value | 4.980 | 4.772 | 2.096 | 0.484 | 0.103 | 0.617 | 3.308 | 8.114 |
| | st.deviation | 0.127 | 0.199 | 0.061 | 0.022 | 0.007 | 0.004 | 0.169 | 0.389 |
| *B-FRAM* | mean value | 2.768 | 2.391 | 1.873 | 0.525 | 0.267 | 0.244 | 0.760 | 3.234 |
| | st.deviation | 0.148 | 0.225 | 0.138 | 0.041 | 0.013 | 0.030 | 0.096 | 0.151 |
| *B-Ref + RAP* | mean value | 3.288 | 4.370 | 4.620 | 1.494 | 0.042 | 0.223 | 0.106 | 2.468 |
| | st.deviation | 0.022 | 0.105 | 0.011 | 0.117 | 0.002 | 0.010 | 0.020 | 0.142 |
| *B-PmB + RAP* | mean value | 4.430 | 4.711 | 4.209 | 1.155 | 0.108 | 0.276 | 0.936 | 2.794 |
| | st.deviation | 0.327 | 0.275 | 0.032 | 0.100 | 0.005 | 0.008 | 0.050 | 0.031 |
| *B-FRAM + RAP* | mean value | 2.500 | 3.291 | 3.229 | 1.094 | 0.031 | 0.201 | 0.088 | 2.398 |
| | st.deviation | 0.350 | 0.122 | 0.004 | 0.028 | 0.001 | 0.020 | 0.002 | 0.131 |
| *T-Ref.* | mean value | 2.698 | 3.189 | 2.924 | 0.536 | 0.075 | 0.144 | 1.092 | 4.215 |
| | st.deviation | 0.077 | 0.231 | 0.093 | 0.032 | 0.021 | 0.015 | 0.012 | 0.343 |
| *T-FRAM* | mean value | 2.073 | 2.607 | 2.507 | 0.698 | 0.093 | 0.163 | 0.141 | 1.423 |
| | st.deviation | 0.124 | 0.124 | 0.038 | 0.009 | 0.002 | 0.021 | 0.006 | 0.111 |

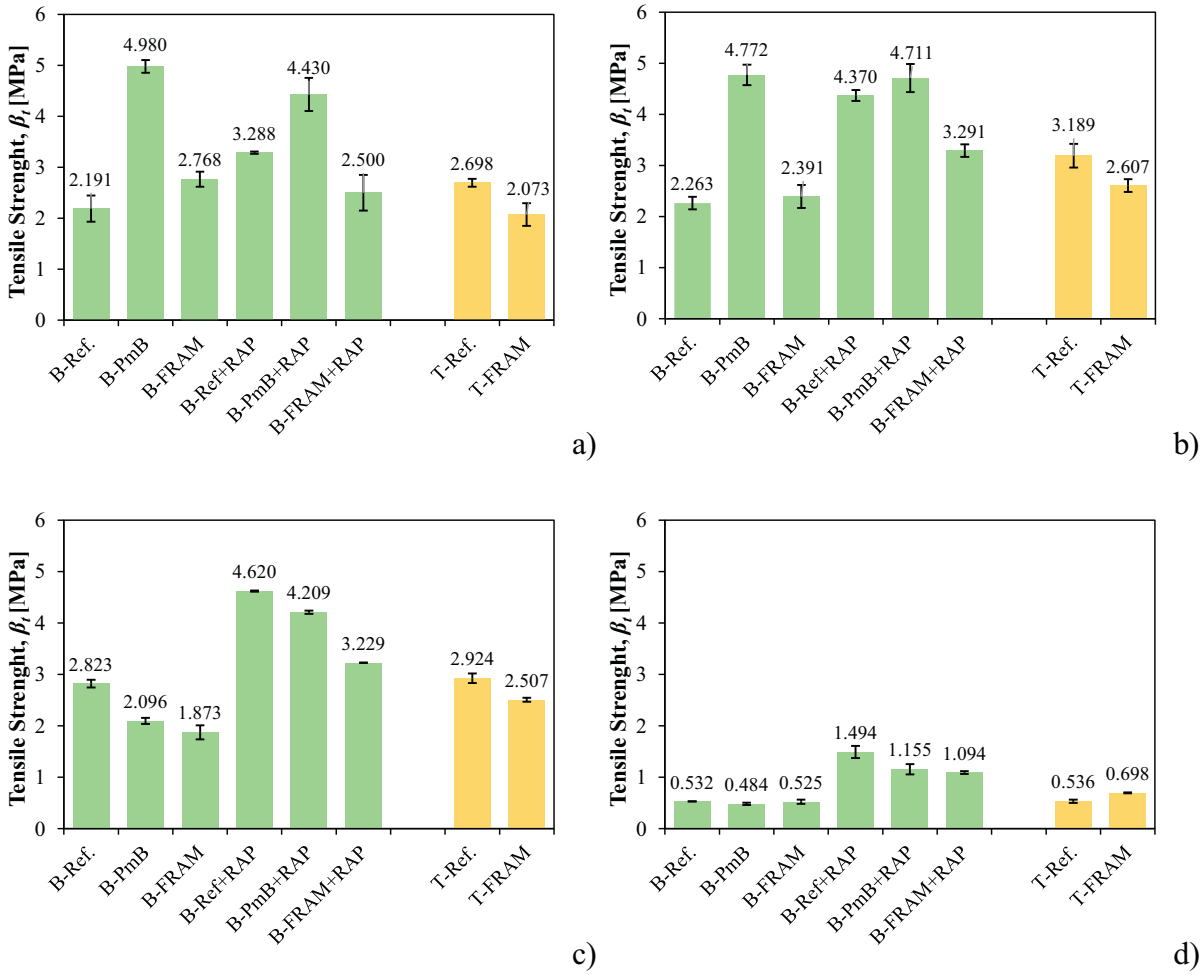


**Fig. 8.** UTST results and the standard deviation for a) tensile strength at −25 °C; b) tensile strength at −10 °C; c) tensile strength at 5 °C; d) tensile strength at 20 °C; e) tensile failure strain at −25 °C; e) tensile failure strain at −10 °C; g) tensile failure strain at 5 °C; and h) tensile failure strain at 20 °C.

## 5. Results and analyses

### 5.1. Thermal stress restrained specimen test (TSRST) results

Fig. 6 shows the thermal stress evolution over the temperature $\sigma_{cry}(T)$ for the different groups of mixtures. The mean values of three replicates for each mixture are reported. It can be noticed that the curves corresponding to the FRAM mixtures are always lower (except for the Porous Aspahlt mixture where a plain binder in a higher amount was used and for the base layer mixture where a hard binder is used) than the reference ones. A noticeable increase in the thermal stress starts for all the FRAM mixtures at lower temperatures compared to the ones of the reference mixtures. This trend indicates that FRAM mixtures have a favorable behavior in terms of thermal stress increase over the considered temperature range. It might be hypothesized that this effect is associated with the interaction of binder and fibers and the impact of fibers on the overall mix design. In addition, as shown in Fig. 6a, a limited increase of 0.3% binder content in the mix design of the *S-AC-FRAM* mixture (from *S-AC-FRAM-4.3* to *S-AC-FRAM-4.6*) led to a remarkable improvement of the low temperature performances of the material containing fibers. The *S-AC-FRAM 4.6* can reach higher thermal stresses and much lower failure temperature than *the S-AC-FRAM 4.3*, and similar $\sigma_F$ with the reference mixture but favorably lower failure temperature. From Fig. 6, it is clear also to see the effects of the RAP on the low temperature performances. In fact, all the thermal stress curves of the mixtures containing RAP are shifted upward compared to mixtures containing only fresh materials. This trend can be due to the aged binder of the RAP that affects the performances of all mixtures, exhibiting reduced relaxation and, therefore, more prone to thermal cracking.

Table 4 summarizes all the TSRST results reporting the average fracture temperatures (TF) values and the failure stresses ($\sigma_F$) between three replicates for each mixture. The calculated standard deviation suggests good repeatability of the testing results (Fig. 7). In the case of TSRST, the best performance is associated with the lowest value of failure temperature and the highest value of failure stress.

The mixtures containing fibers do not exhibit low temperature performance comparable to that of the polymer modified materials while showing similar properties to the corresponding reference mixtures. It should be remarked that an increase of only 0.3% in binder content in the surface mixture (*S-AC-FRAM*) leads to a significant improvement in the behavior at low temperature. In fact, in the *S-AC-FRAM-4.6*, the failure temperature decreased by 4 °C, and the failure stress increased almost by 1.2 MPa compared to *S-AC-FRAM-4.3.* This enhanced performance might result from a combination of effects and material contributions. The increase in asphalt binder content can favorably improve fibers' coating, creating a more cohesive matrix in the mastic phase. In addition, this could be beneficial in promoting a more homogeneous distribution of the fibers in the mixture, with a more effective network reinforcement while minimizing the possibility of uncoated aggregate spots.

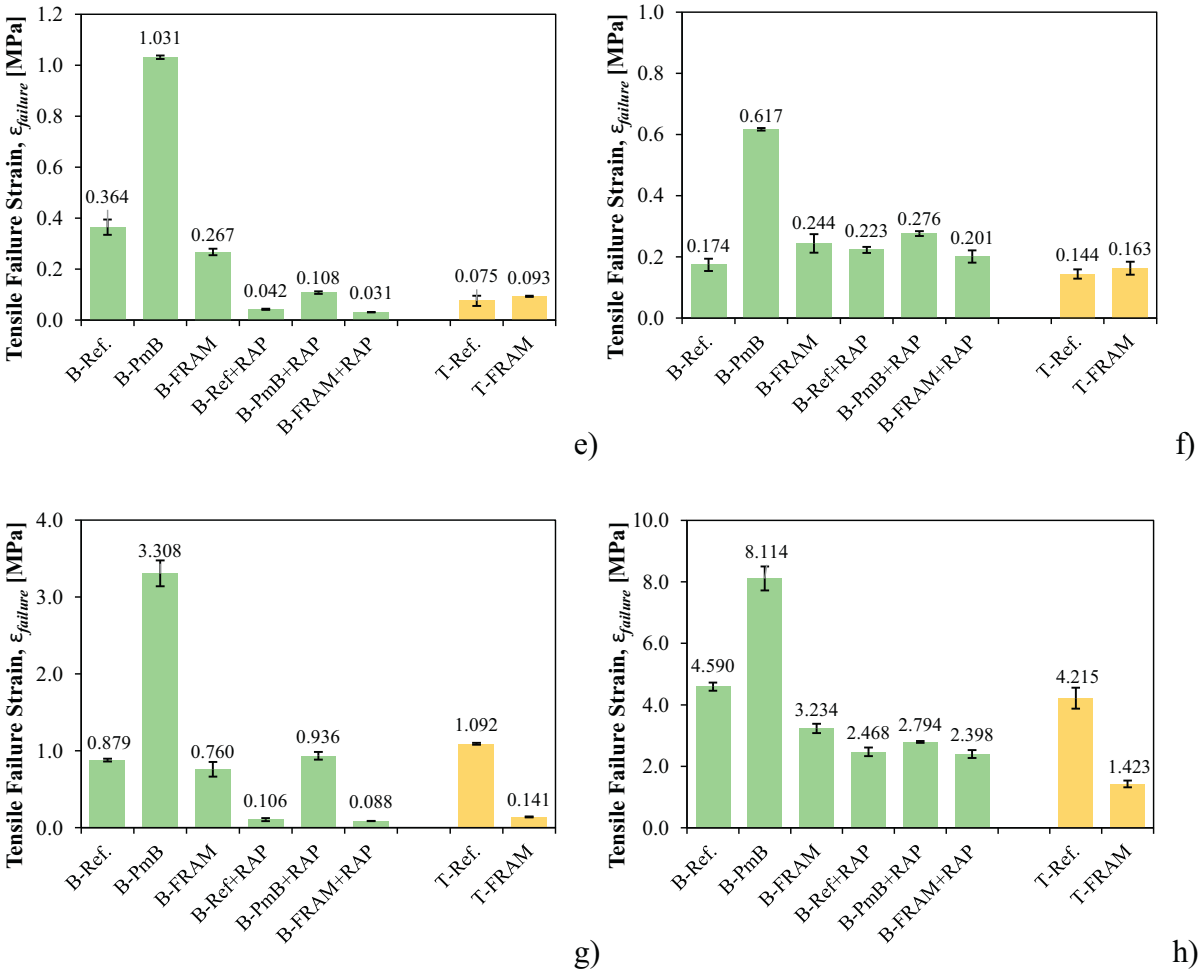


**Fig. 8.** (*continued*).

A lower penetration grade binder (35/50 instead of 50/70) was used for the base layer mixture *T-FRAM*, which negatively affects the low temperature performance. Regarding the mixtures containing RAP, the failure temperatures are higher than for the corresponding mixtures without recycled material due to the negative stiffening effect of the aged RAP binder incorporated in the mixtures at low temperature. In contrast, the failure stresses are overall higher than the corresponding mixtures without RAP. Moreover, based on the category defined in EN 13108–1 (Table 5) and on the cold region classification in Germany (RStO 01, 2012) (Table 6), the corresponding classification for all the mixtures is reported in Table 7.

As shown in Table 7, the *S-PA-FRAM* and the *B-FRAM* with and without RAP present invariably a lower (worse) class in comparison to the corresponding PmB mixures. For the binder layer's mixture, the *B-FRAM* presents a higher (better) class than the reference mixture. Considering the surface layer's mixture, as stated before, the addition of only 0.3% binder content on the *S-AC-FRAM* allows the mixture to reach the highest class with the best low temperature performances. Regarding the base layer's mixtures, the *T-FRAM* shows a lower class than the reference one. Therefore, based on TSRST results, FRAM exhibits moderately better low temperature performances than the reference mixture. However, they are still overperformed by the PmB mixtures.

### 5.2. Uniaxial tension stress test (UTST) results

The strength properties of the binder and base layers' mixtures were tested with the UTST. Unfortunately, for the surface layers' mixtures, not enough samples were produced to obtain reliable results. For each mixture and each temperature, three samples were tested. Table 8 reports the results in terms of tensile strength $\beta_t(T)$, and the corresponding tensile failure strain $\varepsilon_{failure}(T)$ at the testing temperature $T$. The same measurements are visualized in the bar charts in Fig. 8. The tensile strengths and failure strains of the FRAM mixtures are very similar to those of the reference ones and much lower than the PmB mixtures for all investigated temperatures. Therefore, the fibers seem to have no remarkable effect on the strength properties. Moreover, with the addition of RAP, the tensile strength increases, while the failure strain decreases for all the mixtures comparing the results at a constant temperature (only some exceptions for the tensile strength can be detected at the lowest temperature − 25 °C) and this trend is more visible as the temperature increases.

Fig. 9 presents the curves of the tensile strength, tensile failure strain, and the tensile strength reserve versus temperature for the binder and base layers' mixtures with and without RAP. Figs. 8a) and b) show that the tensile strength values increased until they reached their peak values as the temperature decreased. For both sets of binder layers' mixtures (with and without RAP) and the base layers' mixture tested at a temperature of +20 °C, the tensile strength was almost the same, presenting higher values for the mixtures containing RAP. At the temperature of +5 °C, the asphalt mixtures containing RAP and the 50/70 binder showed higher tensile strength values, while the FRAM mixtures always presented the lowest values; these measurements were very similar to the PmB data in the case of the binder layer's mixture designed with fresh materials. Further lowering of the temperature caused a significant

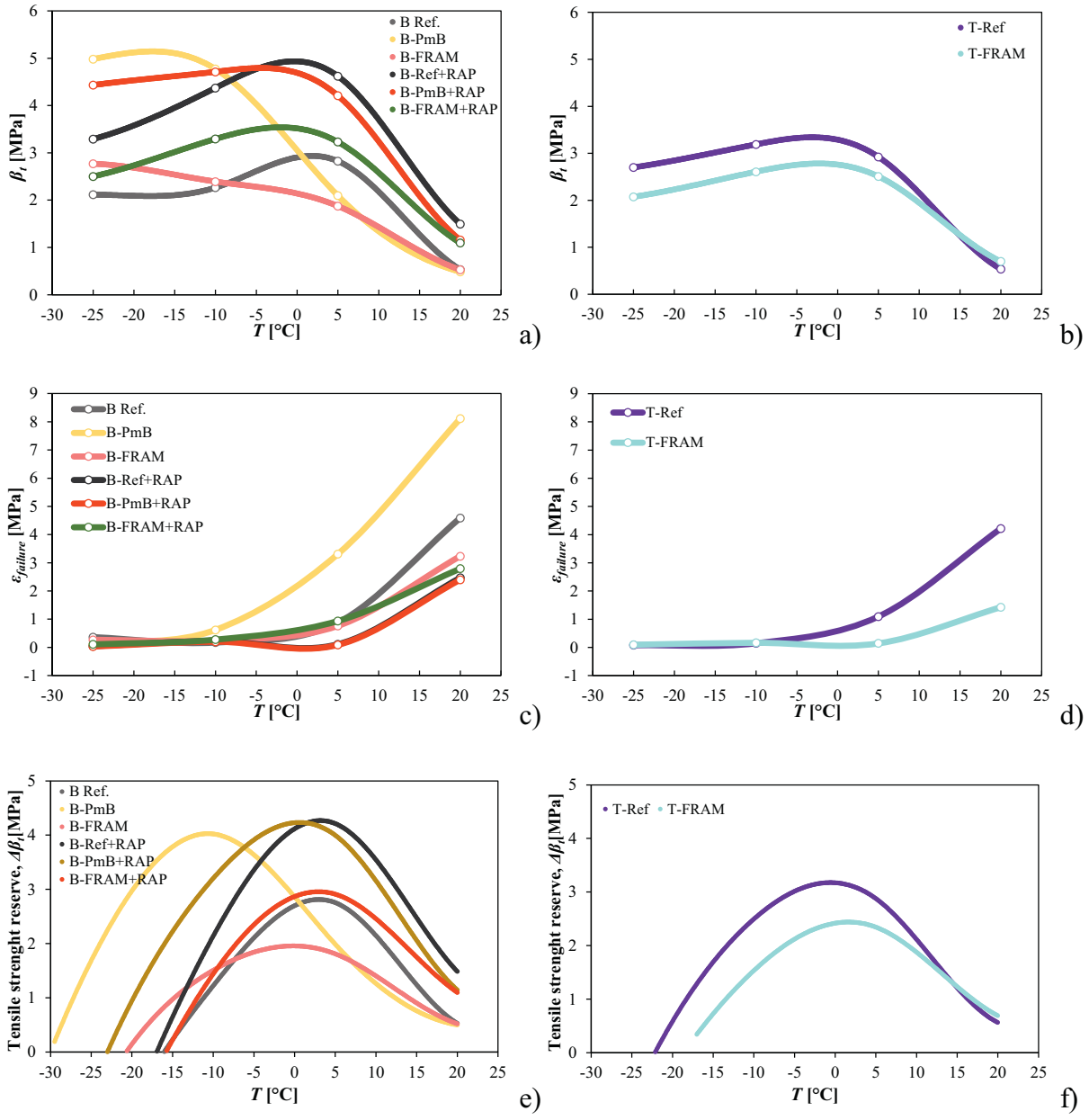


**Fig. 9.** Tensile strength versus temperature for a) binder layers' mixtures with and without RAP; b) base layers' mixture; Tensile failure strain versus temperature for c) binder layers' mixtures with and without RAP; d) base layers' mixture; Tensile strength reserve versus temperature for e) binder layers' mixtures with and without RAP; f) base layers' mixture.

increase in tensile strength of the PmB asphalt mixture compared to asphalt mixtures with neat binders and the FRAM mixtures. At −10 °C and − 20 °C, the FRAM mixtures presented higher tensile strength values than the reference mixtures but significantly lower than the PmB mixtures. According to the literature, low-temperature cracking occurs when thermal tensile stresses exceed the fracture strength of an asphalt pavement layer (Monismith et al., 1965; Jung and Vinson, 1993). The results presented in Figs. 9a) and b) show that PmB increased the tensile strength of the mixture and moved the peak value to a lower temperature. In the case of mixtures without RAP, the peak value changed from about 2.8 MPa at 3 °C, for the B-Ref mixture, to over 5 MPa at the temperature of −17 °C, for the PmB mixture. This enhanced low temperature behavior might be attributed to the premium characteristics of the PmB binder allowing a wider range of relaxation capability together with a reduced brittleness and higher strength. The curve of the *B-FRAM* suggests that this material has still not reached the peak strength value at −25 °C. Therefore, the maximum tensile strength could be located at a lower temperature than the PmB mixture, but its value will be smaller than the PmB mixture and larger than the reference mixture with the neat 50/70. Such a peculiar trend could be the result of the fibers still bridging across the cracks delaying the formation of the final microcrack leading to complete failure while providing a limited strength increment. Considering the base layer mixtures, lowering the temperature, the *T-FRAM* shows lower tensile strength in comparison to the *T-Ref*. Taking into account that the *T-FRAM* is produced with a harder binder, it seems that the fibers at very low temperatures make the mixture softer and more elastic. The failure strain results over testing temperatures are plotted in Fig. 9c) and d). It was observed that the failure strain differentiates the mixtures as the temperature increases in both layers, in particular at a temperature higher than −10 °C. For mixtures prepared with fresh materials, the FRAM mixture achieved lower failure strain. Based on the results of the TSRST and UTST tests, it is possible to

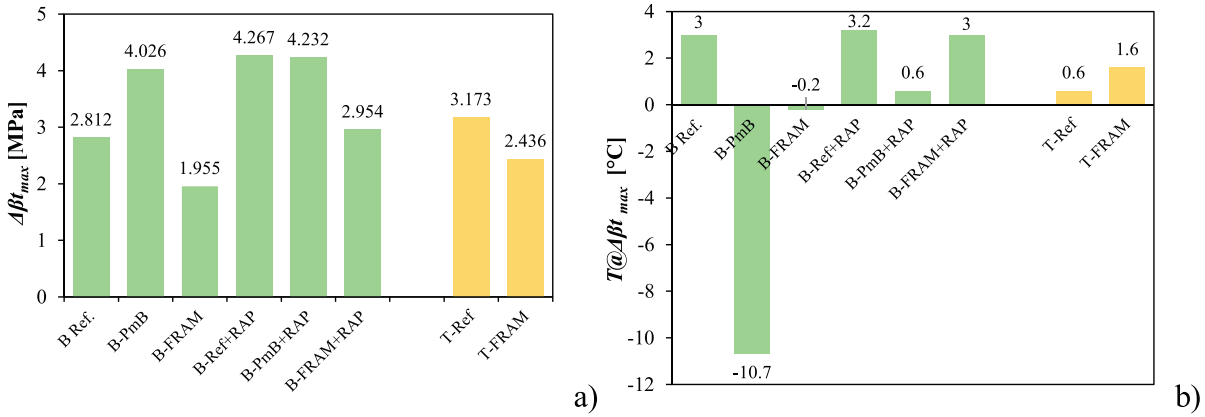


**Fig. 10.** a) Maximum strength reserve results; and (b) the temperature at the maximum value of strength reserve for all the mixtures.

**Table 9**
SCB results at −18 °C.

| Mixtures | $\sigma_{max}$ [MPa] | SD | $G_F$ [J/m$^2$] | SD | $K_{IC}$ [MPa×m$^{0.5}$] | SD | FI [J/m$^2$ × 10$^{-4}$] | SD | CRI [J/m$^2$ × kN] | SD |
|---|---|---|---|---|---|---|---|---|---|---|
| *S-AC Ref.* | 1.032 | 0.139 | 1.187 | 0.167 | 7.619 | 1.032 | 6.208 | 0.562 | 0.284 | 0.013 |
| *S-AC-FRAM 4.3* | 0.898 | 0.013 | 0.896 | 0.156 | 6.647 | 0.090 | 6.465 | 0.351 | 0.219 | 0.023 |
| *S-AC-FRAM 4.6* | 0.953 | 0.031 | 0.954 | 0.190 | 7.112 | 0.291 | 6.298 | 0.444 | 0.214 | 0.009 |
| *S-AC Ref. + RAP(S)* | 0.800 | 0.023 | 0.835 | 0.008 | 6.056 | 0.521 | 3.638 | 0.421 | 0.223 | 0.026 |
| *S-AC-FRAM 4.6 + RAP(S)* | 0.756 | 0.141 | 0.849 | 0.124 | 5.672 | 0.986 | 6.501 | 0.624 | 0.216 | 0.018 |
| *S-PA-PmB* | 0.628 | 0.047 | 1.036 | 0.039 | 4.526 | 0.248 | 18.017 | 1.125 | 0.354 | 0.022 |
| *S-PA-FRAM* | 0.479 | 0.019 | 0.627 | 0.124 | 3.516 | 0.202 | 13.884 | 1.321 | 0.294 | 0.022 |
| *B-Ref* | 0.798 | 0.073 | 0.423 | 0.067 | 5.943 | 0.544 | 0.677 | 0.053 | 0.104 | 0.007 |
| *B-PmB* | 0.929 | 0.033 | 0.871 | 0.196 | 6.787 | 0.202 | 7.149 | 0.652 | 0.215 | 0.018 |
| *B-FRAM* | 0.628 | 0.069 | 0.514 | 0.214 | 4.733 | 0.520 | 4.157 | 0.465 | 0.157 | 0.017 |
| *B-Ref + RAP* | 0.898 | 0.066 | 0.477 | 0.104 | 6.561 | 0.479 | 1.484 | 0.112 | 0.128 | 0.009 |
| *B-PmB + RAP* | 0.970 | 0.031 | 0.557 | 0.023 | 7.242 | 0.213 | 1.225 | 0.135 | 0.143 | 0.008 |
| *B-FRAM + RAP* | 0.831 | 0.119 | 0.585 | 0.015 | 6.169 | 0.978 | 5.207 | 0.465 | 0.177 | 0.011 |
| *T-Ref* | 0.655 | 0.040 | 0.430 | 0.068 | 4.895 | 0.284 | 2.603 | 0.225 | 0.172 | 0.015 |
| *T-FRAM* | 0.660 | 0.073 | 0.391 | 0.055 | 4.834 | 0.529 | 3.145 | 0.228 | 0.151 | 0.016 |

**Table 10**
SCB results at −24 °C.

| Mixtures | $\sigma_{max}$ [MPa] | SD | $G_F$ [J/m$^2$] | SD | $K_{IC}$ [MPa×m$^{0.5}$] | SD | FI [J/m$^2$ × 10$^{-4}$] | SD | CRI [J/m$^2$ × kN] | SD |
|---|---|---|---|---|---|---|---|---|---|---|
| *S-AC Ref.* | 1.119 | 0.053 | 1.261 | 0.007 | 8.223 | 1.003 | 1.030 | 0.091 | 0.252 | 0.022 |
| *S-AC-FRAM 4.3* | 0.870 | 0.006 | 1.242 | 0.168 | 6.570 | 0.826 | 4.569 | 0.512 | 0.321 | 0.028 |
| *S-AC-FRAM 4.6* | 0.972 | 0.008 | 1.186 | 0.051 | 7.028 | 0.006 | 5.093 | 0.523 | 0.269 | 0.019 |
| *S-AC Ref. + RAP(S)* | 0.830 | 0.181 | 1.177 | 0.023 | 6.177 | 0.311 | 1.473 | 0.151 | 0.374 | 0.033 |
| *S-AC-FRAM 4.6 + RAP(S)* | 0.760 | 0.021 | 1.144 | 0.185 | 5.729 | 0.129 | 6.415 | 0.703 | 0.330 | 0.025 |
| *S-PA-PmB* | 0.523 | 0.012 | 0.862 | 0.006 | 4.036 | 0.156 | 24.652 | 1.925 | 0.323 | 0.028 |
| *S-PA-FRAM* | 0.410 | 0.006 | 0.429 | 0.011 | 3.035 | 0.225 | 3.214 | 0.332 | 0.238 | 0.020 |
| *B-Ref* | 0.932 | 0.088 | 0.912 | 0.011 | 6.938 | 0.152 | 6.979 | 0.562 | 0.287 | 0.019 |
| *B-PmB* | 0.945 | 0.065 | 1.364 | 0.095 | 6.892 | 0.452 | 45.467 | 4.325 | 0.497 | 0.042 |
| *B-FRAM* | 0.889 | 0.048 | 0.953 | 0.131 | 6.667 | 0.568 | 13.176 | 1.225 | 0.293 | 0.025 |
| *B-Ref + RAP* | 0.992 | 0.124 | 0.930 | 0.071 | 7.339 | 0.970 | 0.927 | 0.086 | 0.256 | 0.021 |
| *B-PmB + RAP* | 0.967 | 0.086 | 1.110 | 0.003 | 7.195 | 0.614 | 3.679 | 0.333 | 0.316 | 0.026 |
| *B-FRAM + RAP* | 0.984 | 0.146 | 1.252 | 0.049 | 7.261 | 1.153 | 5.588 | 0.621 | 0.345 | 0.029 |
| *T-Ref* | 0.773 | 0.117 | 0.972 | 0.039 | 5.801 | 0.910 | 2.314 | 0.192 | 0.305 | 0.024 |
| *T-FRAM* | 0.615 | 0.077 | 1.242 | 0.127 | 4.494 | 0.593 | 4.593 | 0.452 | 0.429 | 0.035 |

calculate the tensile strength reserve as explained in Section 3.2.2. The strength reserve for all tested asphalt mixtures is visualized in Figs. 8e) and f) for the binder and base layers. The asphalt mixtures with a higher value of strength reserve have better resistance to low-temperature cracking.

There are two indicators of this resistance. One is the maximum value of strength reserve, and the second is the temperature at the maximum value of strength reserve. Both are represented in the bar charts in Fig. 10. The lower the calculated values of temperature, the better the resistance to low-temperature cracking.

The previous figures show that the *B-PmB* presents the best low temperature properties considering both indicators. The *B-FRAM* exhibits the lowest maximum strength reserve and the lowest temperature at which the maximum strength reserve is achieved in comparison to the other mixtures, excluding the *B-PmB*. These characteristics indicate that the *B-FRAM* mixture can bear lower traffic levels but down to lower temperatures. It can be noted that the addition of RAP in all the mixtures increased the maximum strength reserve but increased significantly the temperature at which the maximum strength reserve is achieved. This behavior suggests that the RAP mixtures can bear higher traffic levels but at higher temperatures above 0 °C. For the base layers' mixtures, it can be noted that the *T-FRAM* presents the worst low temperature

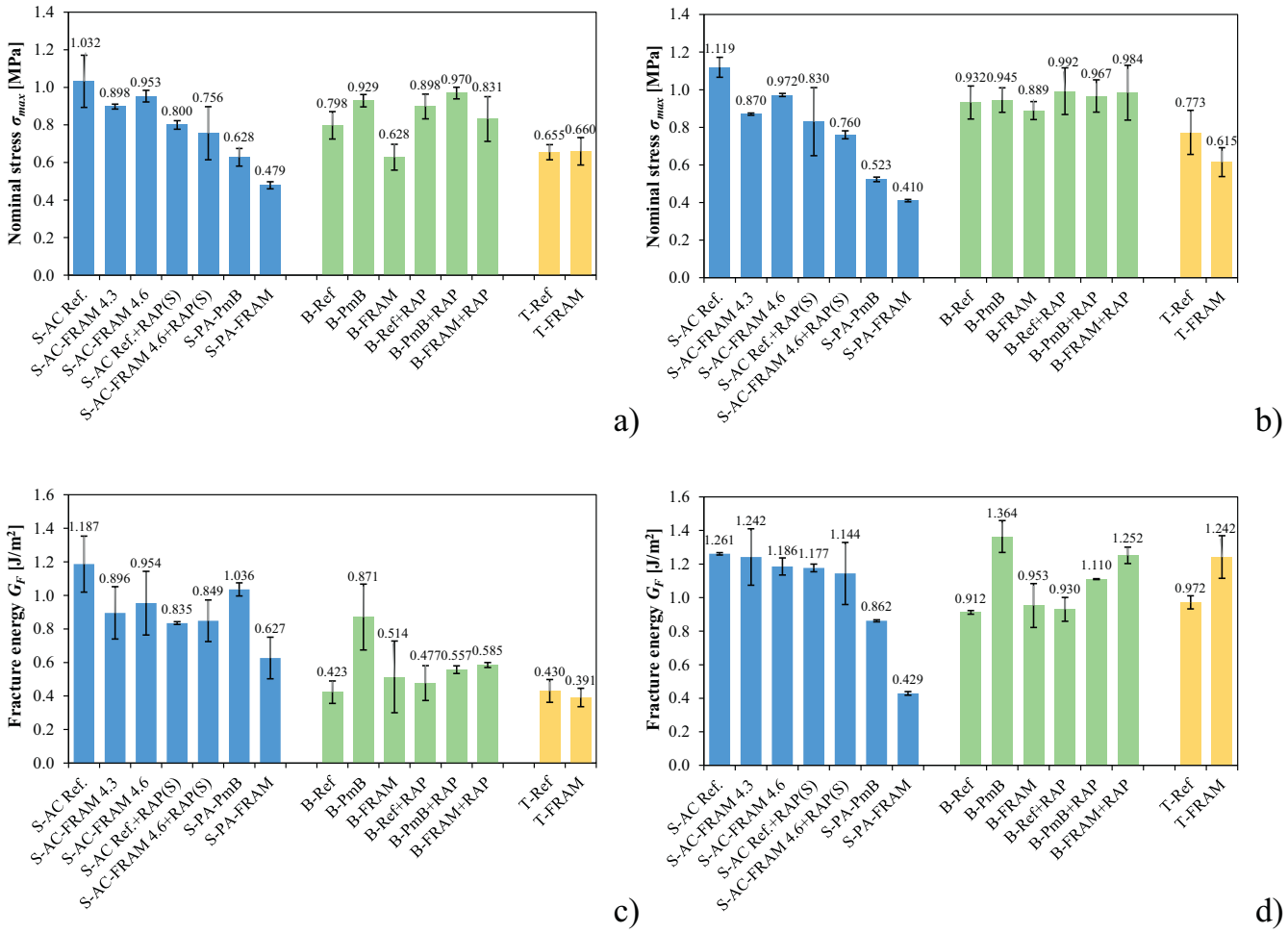


**Fig. 11.** SCB results and the standard deviation for a) nominal stress $\sigma_{max}$ at −18 °C; b) nominal stress $\sigma_{max}$ at −24 °C; c) fracture energy $G_F$ at −18 °C; d) fracture energy $G_F$ at −24 °C; e) fracture toughness $K_{IC}$ at −18 °C; f) fracture toughness $K_{IC}$ at −24 °C; g) Flexibility Index *FI* at −18 °C; h) Flexibility Index *FI* at −24 °C; i) Cracking Resistance Index *CRI* at −18 °C; and j) Cracking Resistance Index *CRI* at −24 °C.

characteristics considering both indicators; however, it should be taken into account that a harder binder is used to produce this mixture.

### 5.3. Semi circular bending test (SCB) results

Tables 9 and 10 summarize the results of the SCB tests in terms of nominal stress, $\sigma_{max}$, fracture energy, $G_F$, and fracture toughness, $K_{IC}$, for all the mixtures under −18 °C and − 24 °C. Three replicates were tested for each condition, and the standard deviation (SD) was calculated for each parameter and condition. The related results together with SD are plotted in Fig. 11 for three different layers under −18 °C and − 24 °C, respectively. Good repeatability (most of the standard deviations are <10%) was observed for all the mixtures, in agreement with previous work (Li, 2005, 2006; Marasteanu et al., 2012; Cannone Falchetto et al., 2017a; Wang et al., 2019).

Concerning the surface layer materials, all the reference mixtures without fibers indicate a relatively higher $\sigma_{max}$, $G_F$ and $K_{IC}$ compared to the fiber reinforced asphalt concrete (AC) and porous asphalt (PA) at both temperatures. The differences between these three parameters are more significant for the mixtures designed with fresh materials at −18 °C. In contrast, the differences are smaller when using recycled materials and at the lower testing temperature of −24 °C, when the material shifts from a quasi-brittle behavior toward increased brittleness (Cannone Falchetto et al., 2014; Cannone Falchetto et al., 2017b). It is worth noting that for AC mixtures prepared with fresh material, a 0.3% binder content increment (S-AC-FRAM 4.6) led to remarkably better thermal fracture resistance than the FRAM prepared with 4.3% binder (S-AC-FRAM 4.3). However, the values are still lower than the reference mixture (S-AC-Ref.). For *FI* and *CRI*, there are only limited differences among different AC mixtures at −18 °C, while FRAM exhibits better fracture properties at −18 °C, especially for mixtures containing RAP. However, for PA mixture, both FI and CRI indicate that the FRAM were unable to achieve the similar properties of reference materials under −18 °C and − 24 °C. Hence, for the surface layer (AC and PA), mixtures prepared without fiber could overall achieve better low temperature resistance performance before and after the macro cracking occurs. A modified mix design could potentially lead to remarkably better thermal fracture properties; this trend associated with a higher binder content (from 4.3% to 4.6%) was also observed in the TSRST results.

For the binder layers' materials at −18 °C, the PmB mixtures (*B-PmB*, *B-PmB + RAP*) showed the highest $\sigma_{max}$, $K_{IC}$, *FI* and *CRI*, followed by the materials produced with plain binders (*B-Ref, B-Ref + RAP*). In contrast, the fiber reinforced asphalt mixtures (*B-FRAM*, *B-FRAM + RAP*) presented the lowest values, which means that the FRAM mixtures obtained the worst cracking resistance before the macro cracking. A closer observation indicates an overall increment of $\sigma_{max}$ and $K_{IC}$ when RAP was added; such a result is more remarkable for *B-FRAM + RAP*. Concerning fracture energy, $G_F$, both reference mixtures (*B-Ref*, *B-Ref + RAP*) showed the lowest value among all the six mixtures. On the other hand, *B-PmB* and *B-FRAM + RAP* present the highest $G_F$. It has to be

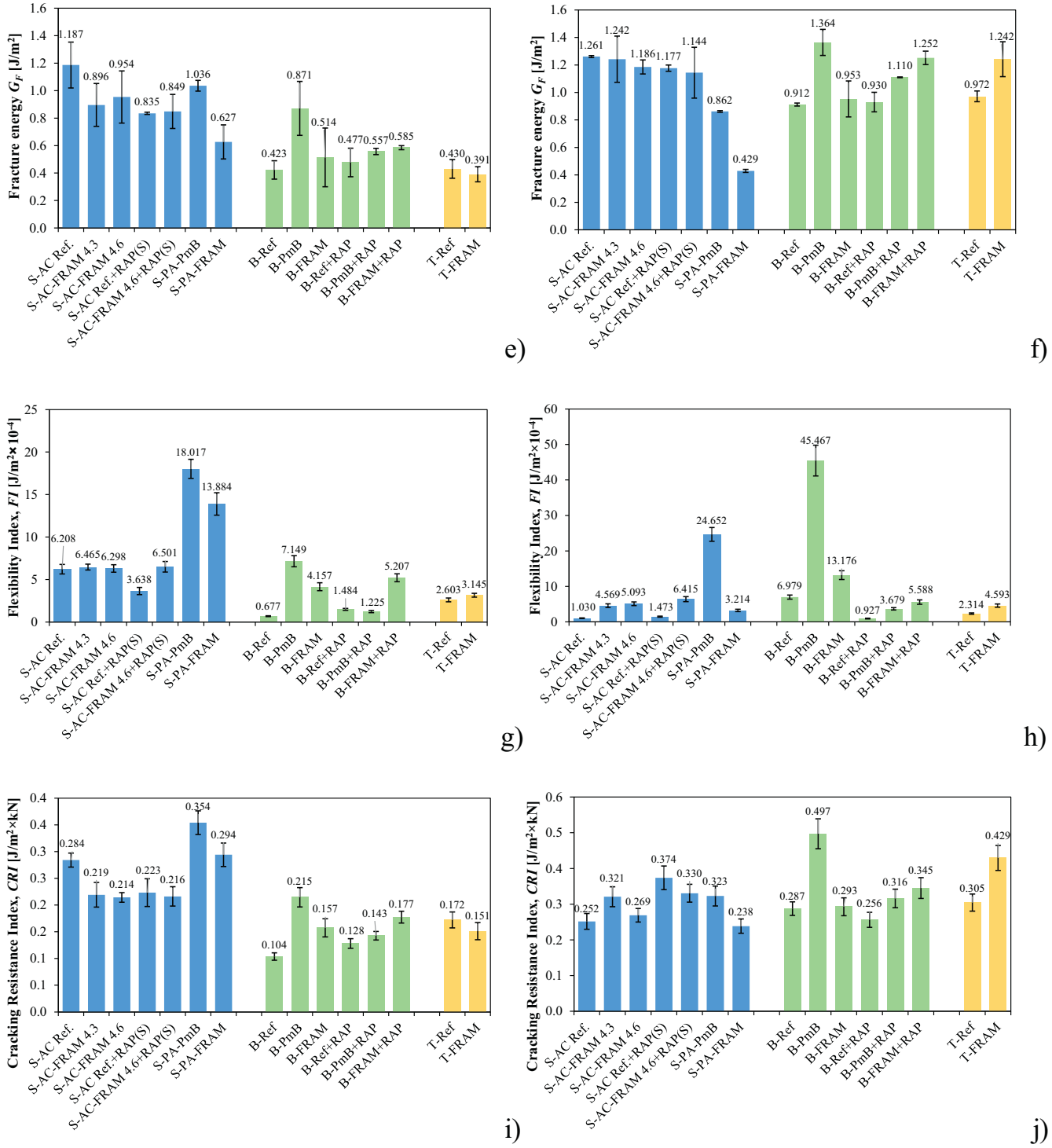


**Fig. 11.** (*continued*).

highlighted that the addition of RAP (*B-PmB + RAP*) decreased $G_F$, while mixtures *B-Ref + RAP* and *B-FRAM + RAP* showed similar fracture energy. The differences of $\sigma_{max}$, $K_{IC}$, and $G_F$ among the mixtures containing RAP are smaller than for fresh materials; this trend is consistent with what was observed for the surface layer mixtures. In the case of $T$ = -24 °C, FRAM mixtures exhibited a comparable response to the corresponding reference mixtures and showed to be superior to the PmB material before the macro cracking occurred. This behavior is supported by the overall post-peak curves and *FI* indicating overall less brittle characteristics most likely associated with a beneficial effect of incorporation of fibers.

For the base layer mixtures, all three cracking parameters did not present substantial differences at −18 °C. On the contrary, slightly lower peak stress at macro cracking, together with remarkably better overall fracture resistance (larger $G_F$ compared to the reference mixture), was observed for FRAM at −24 °C. This behavior might be due to the addition of fibers to a mixture composed with a hard 35/50 binder that can lead to similar fracture resistance to the one of the reference mixture composed with a traditional 50/70 binder.

To better understand the low temperature fracture behavior between

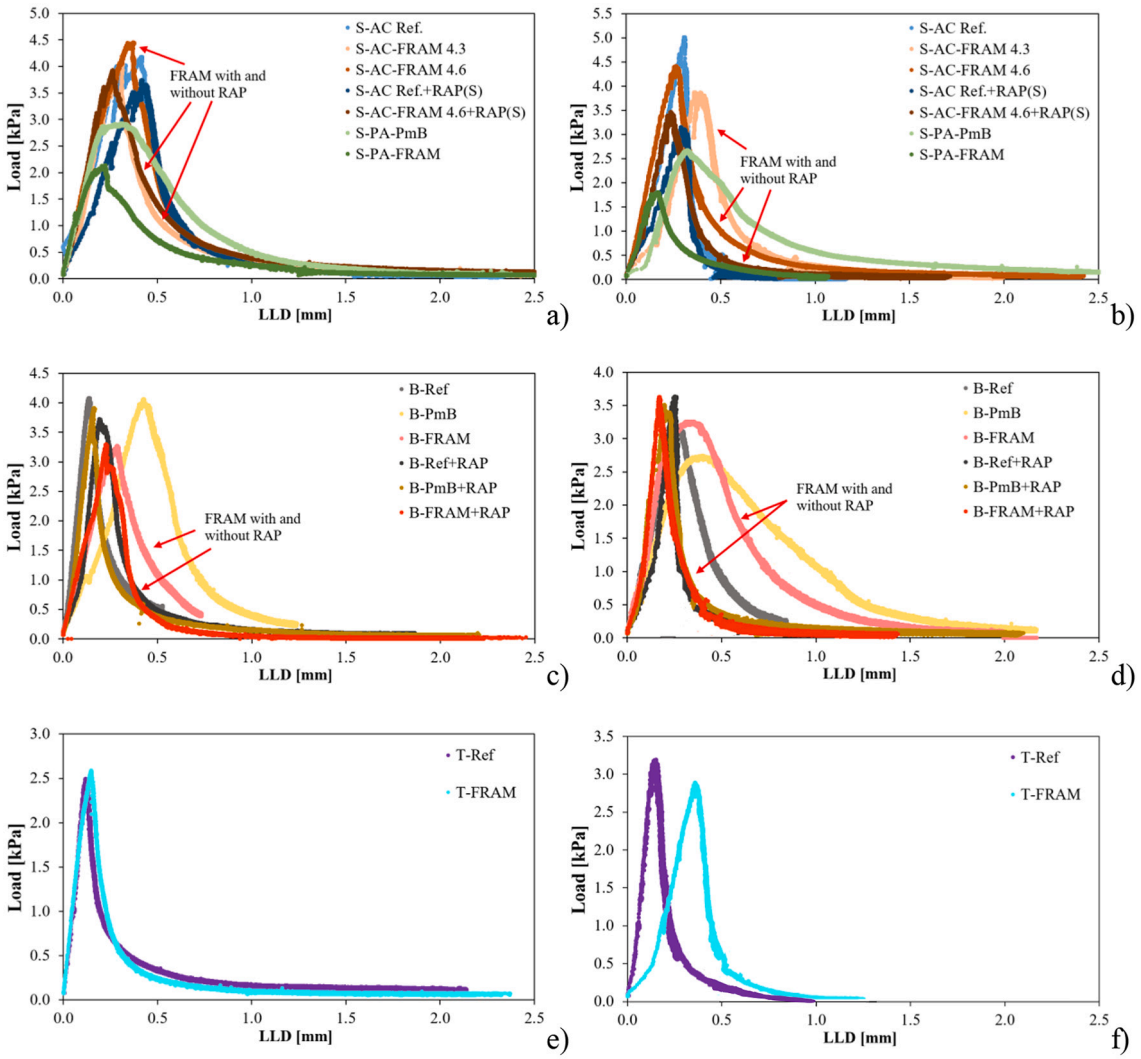


**Fig. 12.** Comparison curves of load vs. LLD for a) surface layer at −18 °C; b) surface layer at −24 °C; c) binder layer at −18 °C; d) binder layer at −24 °C; e) base layer at −18 °C; f) base layer at −24 °C.

different mixtures, load vs. LLD curves were plotted for each material and visualized in Fig. 12. For fresh AC and PA mixture in the surface layer at −18 °C, all mixtures indicate very similar pre-peak slopes. S-AC-FRAM 4.3 and S-AC-FRAM 4.6 also achieved comparable or higher peak load compared to S-AC-Ref., while S-PA-FRAM attained a much lower peak load than the one without fiber (S-PA-PmB). However, this trend is not the case at −24 °C. A relatively gradual pre-peak slope is observed in S-AC-FRAM, and an overall lower peak load is achieved in all the FRAM mixtures compared to the reference ones. For AC mixtures prepared with RAP, a steep pre-peak slope and gentle decreased post-peak curves are observed in the FRAM (S-AC-FRAM 4.6 + RAP(S)) at both testing temperatures. Considering the value of $G_F$ listed in Tables 9 and 10, the use of fiber and different mix designs have limited influence on the fracture properties of AC mixtures under two different testing temperatures, while the use of fiber in PA mixture is unable to achieve the properties of mixtures prepared with polymer modified binder.

In the case of binder layers, B-PmB indicates the most gentle pre-peak and post-peak. Hence, even though the peak load of B-PmB is much lower than the other two mixtures at −24 °C, this does not affect B-FRAM to obtain the highest $G_F$ values, which means the best anti-fracture performance. For B-FRAM, its curve and $G_F$ values are both between B-PmB and B-Ref. Hence, the use of fiber could improve the fracture properties of mixtures prepared with a plain binder; however, it is unable to achieve the one produced with PmB. For mixtures prepared with RAP, only limited differences could be observed in the curves among these three materials. Therefore, the use of RAP vanished the differences caused by fiber and PmB binders. Further studies will be conducted to better understand the effects of RAP in FRAM at low temperatures. Considering the $G_F$ values and the shape of the curves, the use of fiber could lead to a relative plastic behavior; however, they are unable to achieve the performance as PmB mixture. The combined use of fiber and RAP ultimately results in the best anti-fracture performance among all the different mixtures. Such trends are valid for different temperatures.

Very similar curves and GF values are found for the base layer at −18 °C. In the case of −24 °C, a much gentle pre-peak and post-peak slope and higher $G_F$ value are observed in T-FRAM compared to T-Ref. Hence, the use of fiber in the base layer could lead to better anti-fracture properties, especially at very low temperatures. In conclusion, the use of fiber could positively influence the fracture properties for binder and base layer mixtures; however, only limited benefits could be observed in case of the surface layer.

## 6. Summary and conclusions

The present study addressed the effects of fibers and Reclaimed Asphalt Pavement (RAP) on low temperature performance of four different asphalt mixture types. Dense mixtures for surface, binder, and

base layers were designed to incorporate polyacrylonitrile fibers, while aramid and polyolefins fibers were combined to prepare a porous mixture for surface layer. The experimentation consisted of three types of tests: Thermal Stress Restrained Specimen, Uniaxial Tension Stress, and Semi-Circular Bending. Based on the testing campaign and the analysis performed, the following conclusions can be drawn:

- From the TSRST results, adding fibers improves the relaxation response of the mixtures compared to the reference ones. The FRAM mixtures presented similar or moderately better failure temperatures and failure stresses than the reference ones; however, they cannot provide the high performance of the studied PmB mixtures.
- The addition of only 0.3% in binder content led to a remarkable improvement in the low temperature performances of the FRAM mixtures. This effect can be due to the better fibers' coating, which generates a more cohesive matrix in the mastic phase and promotes a more homogeneous distribution of the fibers in the mixture, with a more effective network reinforcement, minimizing the possibility of uncoated aggregate spots.
- Based on the UTST results, the fibers seem to have no remarkable effects on the tensile strength and tensile failure strain. However, looking at the tensile strength curves, the FRAM mixtures present a peak value of the tensile strength at a lower temperature than the reference and PmB mixtures, with a lower value than the PmB, but higher than the reference one. This trend can be explained as a result of the fibers bridging across the crack and delaying the formation of the final microcracks.
- Combining the results of TSRST and UTST, it can be concluded that the *B-FRAM* exhibits the lowest maximum strength reserve and the lowest temperature at which the maximum strength reserve is achieved in comparison to the other mixtures, excluding the *B-PmB*. These characteristics indicate that the B-FRAM mixture can bear lower traffic levels but down to lower temperatures than conventional mixtures.
- The SCB facture parameters provide a more complex vision of the behavior of the materials investigated. Before the crack occurs, the PmB mixtures exhibit the best response; while fibers are not delivering such a level of performance, they contribute to a substantially higher peak load than mixtures prepared without fibers. Significant benefits in using fibers are obtained in terms of fracture energy and combination with RAP.

It should be noted that, in this study only the optimal fiber content suggested by the producers was used. Follow-up research is recommended to extend the study to a large variety of fibers and at different contents and develop a tailored mix design capable of better accounting for the impact of fibers on the mix design formula. Moreover, due to the limited experimental data set, no statistical analysis was performed in this work. A testing plan with more replicates will be planned in the follow-up study.

## Declaration of Competing Interest

No potential conflict of interest was reported by the authors.

## Data availability

No data was used for the research described in the article.

## Acknowledgments

The financial support of CEDR Project Fostering the implementation of fiber-reinforced asphalt mixtures by ensuring its safe, optimized and cost-efficient use (FIBRA) [Grant Number 867481] is gratefully acknowledged.

## References

AASHTO T394, 2021. Standard Method of Test for Determining the Fracture Energy of Asphalt Mixtures Using the Semicircular Bend Geometry (SCB). American Association of State Highway and Transportation Officials, Washington.

Abtahi, S.M., Sheikhzadeh, M., Hejazi, S.M., 2010. Fiber-reinforced asphalt-concrete–a review. Constr. Build. Mater. 24 (6), 871–877. https://doi.org/10.1016/j.conbuildmat.2009.11.009.

Achilleos, C., Hadjimitsis, D., Neocleous, K., Pilakoutas, K., Neophytou, P.O., Kallis, S., 2011. Proportioning of steel fibre reinforced concrete mixes for pavement construction and their impact on environment and cost. Sustainability 3 (7), 965–983. https://doi.org/10.3390/su3070965.

Al-Qudsi, A., Cannone Falchetto, A., Wang, D., Büchler, S., Kim, Y.S., Wistuba, M.P., 2020. Finite element cohesive fracture modeling of asphalt mixture based on the semi-circular bending (SCB) test and self-affine fractal cracks at low temperatures. Cold Reg. Sci. Technol. 169, 102916 https://doi.org/10.1016/j.coldregions.2019.102916.

Aurangzeb, Q., Al-Qadi, I.L., Ozer, H., Yang, R., 2014. Hybrid life cycle assessment for asphalt mixtures with high RAP content. Resour. Conserv. Recycl. 83, 77–86. https://doi.org/10.1016/j.resconrec.2013.12.004.

Bayomy, F., Muftah, A., Wen, H., Bahadori, A., 2016. Evaluation of Fiber-Reinforced Asphalt Pavements: Laboratory Study (No. FHWA-ID-16-237). Transportation Dept, Idaho.

Büchler, S., Cannone Falchetto, A., Walther, A., Riccardi, C., Wang, D., Wistuba, M.P., 2018. Wearing course mixtures prepared with high reclaimed asphalt pavement content modified by rejuvenators. Transp. Res. Rec. 2672 (28), 96–106. https://doi.org/10.1177/0361198118773193.

Bueno, M., Poulikakos, L.D., 2020. Chemo-mechanical evaluation of asphalt mixtures reinforced with synthetic fibers. Front. Built Environ. 6, 41. https://doi.org/10.3389/fbuil.2020.00041.

Cannone Falchetto, A., Le, J.L., Turos, M.I., Marasteanu, M.O., 2014. Indirect determination of size effect on strength of asphalt mixtures at low temperatures. Mater. Struct. 47 (1), 157–169.

Cannone Falchetto, A., Moon, K.H., Lee, C.B., Wistuba, M., 2017a. Correlation of low temperature fracture and strength properties between SCB and IDT tests using a simple 2D FEM approach. Road Mater. Pavement Des. 18 (2), 329–338. https://doi.org/10.1080/14680629.2017.1304258.

Cannone Falchetto, A., Wistuba, M.P., Marasteanu, M.O., 2017b. Size effect in asphalt mixture at low temperature: types I and II. Road Mater. Pavement Des. 18 (sup1), 235–257. https://doi.org/10.1080/14680629.2016.1266764.

Cannone Falchetto, A., Moon, K.H., Wang, D., Riccardi, C., Wistuba, M.P., 2018. Comparison of low-temperature fracture and strength properties of asphalt mixture obtained from IDT and SCB under different testing configurations. Road Mater. Pavement Des. 19 (3), 591–604. https://doi.org/10.1080/14680629.2018.1418722.

EAPA, 2022. Asphalt in Figures – Provisional Figures 2021. https://eapa.org/asphalt-in-figures/. Accessd in 19.10.2022.

EN 12591, 2015. Binder and Bituminous Binders. Specifications for Paving Grade Binders. European Committee for Standardization.

EN 12697-2, 2013. Bituminous Mixtures. Test Methods. Determination of Particle Size Distribution. European Committee for Standardization.

EN 12697-3, 2013. Bituminous Mixtures. Test Methods. Binder Recovery: Rotary Evaporator. European Committee for Standardization.

EN 12697-44, 2019. Bituminous Mixtures. Test Methods. Crack Propagation by Semi-Circular Bending Test. European Committee for Standardization, Brussels.

EN 12697-46, 2012. Bituminous Mixtures. Test Methods. Test Methods for Hot Mix Asphalt, Low Temperature Cracking and Properties by Uniaxial Tension Tests. European Committee for Standardization, Brussels.

EN 12697-5, 2019. Bituminous Mixtures. Test Methods. Determination of the Maximum Density. European Committee for Standardization.

EN 13108-1, 2016. Bituminous Mixtures. Material Specifications. Asphalt Concrete. European Committee for Standardization.

EN 14023, 2010. Binder and Bituminous Binders. Specification Framework for Polymer Modified Binders. European Committee for Standardization.

EN 933-1, 2012. Tests for Geometrical Properties of Aggregates - Part 1: Determination of Particle Size Distribution - Sieving Method. European Committee for Standardization.

Fakhri, M., Hosseini, S.A., 2017. Laboratory evaluation of rutting and moisture damage resistance of glass fiber modified warm mix asphalt incorporating high RAP proportion. Constr. Build. Mater. 134, 626–640. https://doi.org/10.1016/j.conbuildmat.2016.12.168.

Gupta, A., Rodriguez-Hernandez, J., Castro-Fresno, D., 2019. Incorporation of additives and fibers in porous asphalt mixtures: a review. Materials 12 (19), 3156. https://doi.org/10.3390/ma12193156.

Hugener, M., Wang, D., Cannone Falchetto, A., Porot, L., Kara De Maeijer, P., Orešković, M., Tebaldi, G., 2022. Recommendation of RILEM TC 264 RAP on the evaluation of asphalt recycling agents for hot mix asphalt. Mater. Struct. 55 (2), 1–9. https://doi.org/10.1617/s11527-021-01837-0.

Jung, D., Vinson, T.S., 1993. Low temperature cracking resistance of asphalt concrete mixtures. J. Assoc. Asph. Paving Technol. 62, 54–92.

Kaloush, K.E., Biligiri, K.P., Zeiada, W.A., Rodezno, M.C., Reed, J.X., 2010. Evaluation of fiber-reinforced asphalt mixtures using advanced material characterization tests. J. Test. Eval. 38 (4), 400–411. https://doi.org/10.1520/jte102442.

Kim, Y.S., Cannone Falchetto, A., Wang, D., Cheraghian, G., Poulikakos, L.D., Bueno, M., Büchner, J., 2020. Experimental Investigation on the Effect of Fibers on the Mechanical Properties of Asphalt Mortar at Intermediate and High Temperature. Transportation Research Board (TRB) (No. 19-02810), Washington, D.C.

Li, X., 2005. Investigation of the Fracture Resistance of Asphalt Mixtures at Low Temperatures with a Semi Circular Bend (SCB) Test. Ph.D. Thesis. University of Minnesota, Minneapolis, MN.
Li, X., 2006. Evaluation of the Factors that Affect the Fracture Resistance of Asphalt Mixtures at Low Temperatures Using Mechanical Testing and Acoustic Emission Methods. Ph.D. Thesis. University of Minnesota, Minneapolis, MN.
Li, Q., Mills, L., McNeil, S., 2011. The Implications of Climate Change on Pavement Performance and Design. University of Delaware. University Transportation Center.
Mahrez, A., Karim, M.R., Bt Katman, H.Y., 2005. Fatigue and deformation properties of glass fiber reinforced bituminous mixes. J. East. Asia Soc. Transp. Stud. 6, 997–1007. https://doi.org/10.11175/easts.6.997.
Marasteanu, M., Buttlar, W., Bahia, H., Williams, C., Moon, K.H., Teshale, E.Z., Kvasnak, A., 2012. Investigation of low temperature cracking in asphalt pavements national pooled fund study–phase II. In: Research Project Final Report 2012–23.
Ministerio de Fomento, 2010. PG-3 Pliego de Prescripciones Técnicas Generales Para Obras de Carreteras y Puentes. Ediciones Liteam SL, Madrid, Spain (In Spanish).
Moghaddam, T.B., Soltani, M., Karim, M.R., 2014. Evaluation of permanent deformation characteristics of unmodified and polyethylene terephthalate modified asphalt mixtures using dynamic creep test. Mater. Des. 53, 317–324.
Monismith, C.L., Secor, G.A., Secor, K.E., 1965. Temperature induced stresses and deformations in asphalt concrete. J. Assoc. Asph. Paving Technol. 34, 248–285.
Morea, F., Zerbino, R., 2018. Improvement of asphalt mixture performance with glass macro-fibers. Constr. Build. Mater. 164, 113–120. https://doi.org/10.1016/j.conbuildmat.2017.12.198.
Muftah, A., Bahadori, A., Bayomy, F., Kassem, E., 2017. Fiber-reinforced hot-mix asphalt: Idaho case study. Transp. Res. Rec. 2633 (1), 98–107. https://doi.org/10.3141/2633-12.
Office, J.E., Chen, J., Dan, H., Ding, Y., Gao, Y., Guo, M., Zhu, X., 2021. New innovations in pavement materials and engineering: a review on pavement engineering research 2021. J. Traffic Transp. Eng. (Engl. Ed.) 8 (6), 815–999. https://doi.org/10.1016/j.jtte.2021.10.001.
Park, P., El-Tawil, S., Park, S.Y., Naaman, A.E., 2015. Cracking resistance of fiber reinforced asphalt concrete at −20°C. Constr. Build. Mater. 81, 47–57. https://doi.org/10.1016/j.conbuildmat.2015.02.005.
Punith, V.S., Veeraragavan, A., 2011. Characterization of OGFC mixtures containing reclaimed polyethylene fibers. J. Mater. Civ. Eng. 23 (3), 335–341. https://doi.org/10.1061/(asce)mt.1943-5533.0000162.
RStO 01, 2012. Richtlinien für die Standardisierung des Oberbaues von Verkehrsflächen. FGSV Verlag (In German).
Slebi-Acevedo, C.J., Lastra-González, P., Pascual-Muñoz, P., Castro-Fresno, D., 2019. Mechanical performance of fibers in hot mix asphalt: a review. Constr. Build. Mater. 200, 756–769. https://doi.org/10.1016/j.conbuildmat.2018.12.171.
Slebi-Acevedo, C.J., Lastra-Gonzalez, P., Castro-Fresno, D., Bueno, M., 2020a. An experimental laboratory study of fiber-reinforced asphalt mortars with polyolefin-aramid and polyacrylonitrile fibers. Constr. Build. Mater. 248, 118622 https://doi.org/10.1016/j.conbuildmat.2020.118622.
Slebi-Acevedo, C.J., Lastra-González, P., Indacoechea-Vega, I., Castro-Fresno, D., 2020b. Laboratory assessment of porous asphalt mixtures reinforced with synthetic fibers. Constr. Build. Mater. 234, 117224.
Slebi-Acevedo, C.J., Pascual-Muñoz, P., Lastra-González, P., Castro-Fresno, D., 2021. A multi-criteria decision-making analysis for the selection of fibres aimed at reinforcing asphalt concrete mixtures. Int. J. Pavement Eng. 22 (6), 763–779. https://doi.org/10.1080/10298436.2019.1645848.
TL Asphalt-StB 07/13, 2013. Technische Lieferbedingung für Asphaltmischgut für den Bau von Verkehrsflächenbefestigung. FGSV Verlag (In German).
Wang, X., Qiu, Y.J., Xue, S.Y., Yang, Y., Zheng, Y., 2018. Study on durability of high-modulus asphalt mixture based on TLA and fibre composite modification technology. Int. J. Pavement Eng. 19 (10), 930–936. https://doi.org/10.1080/10298436.2016.1224411.
Wang, D., Cannone Falchetto, A., Moon, K.H., Riccardi, C., Pei, J., Wen, Y., 2019. Artificially prepared reclaimed asphalt pavement (RAP)—an experimental investigation on re-recycling. Environ. Sci. Pollut. Res. 26 (35), 35620–35628. https://doi.org/10.1007/s11356-019-05970-w.
Wang, D., Riccardi, C., Jafari, B., Falchetto, A.C., Wistuba, M.P., 2021. Investigation on the effect of high amount of Re-recycled RAP with warm mix asphalt (WMA) technology. Constr. Build. Mater. 312, 125395 https://doi.org/10.1016/j.conbuildmat.2021.125395.
Wu, Z., Zhang, C., Xiao, P., Li, B., Kang, A., 2020. Performance characterization of hot mix asphalt with high RAP content and basalt fiber. Materials 13 (14), 3145. https://doi.org/10.3390/ma13143145.
Xu, Q., Chen, H., Prozzi, J.A., 2010. Performance of fiber reinforced asphalt concrete under environmental temperature and water effects. Constr. Build. Mater. 24 (10), 2003–2010. https://doi.org/10.1016/j.conbuildmat.2010.03.012.
Yan, C., Zhang, Y., Bahia, H.U., 2020. Comparison between SCB-IFIT, un-notched SCB-IFIT and IDEAL-CT for measuring cracking resistance of asphalt mixtures. Constr. Build. Mater. 252, 119060.
Zegeye, E., 2012. Low-Temperature Fracture Behavior of Asphalt Concrete in Semi-Circular Bend Test (Ph.D. Thesis). University of Minnesota, Minneapolis, MN.
Ziari, H., Aliha, M.R.M., Moniri, A., Saghafi, Y., 2020. Crack resistance of hot mix asphalt containing different percentages of reclaimed asphalt pavement and glass fiber. Constr. Build. Mater. 230, 117015 https://doi.org/10.1016/j.conbuildmat.2019.117015.
Ziari, H., Orouei, M., Divandari, H., Yousefi, A., 2021. Mechanical characterization of warm mix asphalt mixtures made with RAP and para-fiber additive. Constr. Build. Mater. 279, 122456 https://doi.org/10.1016/j.conbuildmat.2021.122456.